DEUTSCHES ELEKTRONEN-SYNCHROTRON

DESY 93-112
August 1993


# Physics at $e^+e^-$ Linear Colliders

P. M. Zerwas

*Deutsches Elektronen-Synchrotron DESY, Hamburg*

ISSN 0418-9833

NOTKESTRASSE 85 - 22603 HAMBURG

To be sure that your preprints are promptly included in the
HIGH ENERGY PHYSICS INDEX,
send them to (if possible by air mail):

| | |
|---|---|
| **DESY**<br>**Bibliothek**<br>**Notkestraße 85**<br>**22603 Hamburg**<br>**Germany** | **DESY-IfH**<br>**Bibliothek**<br>**Platanenallee 6**<br>**15738 Zeuthen**<br>**Germany** |

ISSN 0418-9833

DESY 93-112
August 1993

# PHYSICS AT $e^+e^-$ LINEAR COLLIDERS *

P.M. Zerwas
Deutsches Elektronen-Synchrotron DESY
D-22603 Hamburg, FRG

**Abstract**

The physics potential of $e^+e^-$ linear colliders expected to operate in a first phase between 300 and 500 GeV and later at about 2 TeV, is briefly summarized in this report. These machines will enable us to perform precision studies of the top quark and the electroweak gauge bosons. They are ideal instruments to search for Higgs particles and to explore their characteristic properties, in particular in the intermediate mass range. The machines also provide unique opportunities for the investigation of supersymmetric particles. The physics programme of $e^+e^-$ linear colliders is largely complementary to the programme of $pp$ colliders.

*Talk at the Workshop on Physics at Current Accelerators and the Supercollider, Argonne National Laboratory, June 1993

# 1. INTRODUCTION AND SYNOPSIS

## 1.1 The Physical Basis

The search for the fundamental constituents of matter and the exploration of their interactions have been greatly advanced in the past two decades by operating $e^+e^-$ colliders. Joined with the results that have been obtained by other experimental methods, hadron–hadron and lepton–nucleon scattering experiments, a coherent picture of the structure of matter has emerged, that is adequately described by the Standard Model ($\mathcal{SM}$) at a level of unprecedented accuracy.

However, even within the Standard Model a variety of problems remain to be solved.

(i) The mass of the top quark is apparently greater than that of the electroweak gauge bosons. Understanding the role of this particle in Nature is therefore an important goal for the future. The experimental exploration of the $t\bar{t}$ threshold region in $e^+e^-$ collisions will allow the measurement of the top quark mass to better than 500 MeV. This is a desirable goal since future theories of flavor dynamics should provide relations among the fermion masses and mixing angles in which the heavy top quark is expected to play a key rôle. In addition, most stringent tests of the electroweak sector in the Standard Model can be carried out when the top mass is known very accurately. Helicity analyses of the $t\bar{t}$ production vertex and the $t$ decay vertex will determine the magnetic dipole moments of the top quark and the chirality of the $(tb)$ decay current. Bounds on the $\mathcal{CP}$ violating electric dipole moments of the $t$ quark can be set in the same way.

(ii) To study the dynamics of the electroweak gauge bosons is another important task of high energy $e^+e^-$ colliders. The form and the strength of the triple and quartic couplings of these particles are uniquely prescribed by the gauge symmetries in renormalizable theories. The triple gauge boson couplings define the electroweak charges, the magnetic dipole moments and the electric quadrupole moments of the $W^\pm$ bosons in the static limit. By destroying the unitarity cancellations, which in the Standard Model are associated with the longitudinal degrees of freedom of the gauge bosons, any small deviation from the $\mathcal{SM}$ values will be magnified by increasing the energy and the bounds will tighten.

(iii) $e^+e^-$ colliders with an energy between 300 and 500 GeV are ideal instruments to search for Higgs particles throughout the mass range characterized by the scale of electroweak symmetry breaking. The intermediate mass range below $\sim 200$ GeV is theoretically one of the most attractive regions for Higgs masses. In this scenario

Higgs particles remain weakly interacting up to the scale of the grand unification, thus providing a basis for the observed value of the electroweak mixing angle. The Higgs particle can be searched for in several independent production channels, irrespectively of the decay modes. Once the particle is found, its properties must be investigated thoroughly. The external quantum numbers $J^{PC}$ can be verified by analyzing angular correlations in production and decay processes. The Higgs couplings to the $W, Z$ gauge bosons can be determined through the production rates, the couplings to heavy fermions through the Higgs decay branching ratios and Higgs radiation off top quarks. These are fundamental tests of the Higgs mechanism which predicts the couplings to grow with the masses of the particles.

Even though present experimental data support the Standard Model with very high accuracy, extensions can nevertheless be anticipated theoretically. Besides the unification of the gauge symmetries, a very attractive extension of the Standard Model is provided by supersymmetry. This symmetry stabilizes moderate mass values of Higgs particles in the context of very high energy scales as demanded by grand unified theories. Supersymmetry may even build up the physical basis for the Higgs phenomenon itself. This picture is strongly supported by the successful prediction of the electroweak mixing angle in the minimal version of the theory. Many new particles are predicted in such a theory. In the Higgs sector a spectrum of several neutral and charged Higgs bosons, the mass of the lightest Higgs boson being probably less than $\sim$ 150 GeV. The scalar partners of the leptons could have masses in the range of $\sim$ 200 GeV while squarks are expected to be considerably heavier. The lightest supersymmetric states are likely to be fermionic non–colored gaugino/Higgsino states with masses possibly in the 100 GeV range. Searching for these supersymmetric particles will be one of the most important tasks of future colliders.

While new high–mass vector bosons and particles carrying color quantum numbers can be searched for very efficiently at hadron colliders, $e^+e^-$ colliders are in many ways unique in their ability to detect and explore non–colored particles, Higgs bosons, sleptons and many other novel particles [1–3].

## 1.2 Characteristica of Linear Colliders

To avoid prohibitive synchrotron radiation losses, $e^+e^-$ colliders beyond LEPII must be linear machines, a type of accelerator that has been pioneered by the SLC. These machines will probably be realized in two phases. In the first phase the energy range above LEPII up to $\sim$ 500 GeV will be covered, in the second phase an energy of about 1 to 2 TeV will be reached [3–5].



The cross sections of most of the reactions which will be investigated at $e^+e^-$ linear colliders, are of the order of the $\mu$–pair cross section. Given a luminosity $\mathcal{L} = 10^{33}$ cm$^{-2}$ sec$^{-1}$ this leads to about 5,000 $\mu$–pairs per year at a c.m. energy of 500 GeV. To generate the same number of events at higher $e^+e^-$ energies, the luminosity must be scaled up as the square of the energy.

The required high luminosity will be achieved by squeezing the electrons and positrons into bunches of extremely small transverse dimensions, Table 1. Due to the large electromagnetic fields at these small distances, the trajectories of the electrons traversing the positron bunch – and *vice versa* – are bent so that the particles emit synchrotron light during the bunch collisions [*beamstrahlung*]. As a result, a fraction of the electron and positron energies is lost and the initially sharp $e^+e^-$ c.m. energy is slightly smeared out. However, in narrow–band beam designs, these effects can be reduced to a level of a percent and less, not exceeding the intrinsic initial state radiation in any $e^+e^-$ collision process.

| | DLC | NLC | JLC | VLEPP | TESLA | CLIC |
|---|---|---|---|---|---|---|
| c.m. Energy [GeV] | 500 | 500 | 500 | 500 | 500 | 500 |
| Gradient [MV/m] | 17 | 38 | 28 | 96 | 25 | 73/78 |
| Active Length [km] | 30 | 14 | 17 | 6.4 | 20 | 6.6 |
| $\sigma_x^*/\sigma_y^*$ [nm] | 400/33 | 300/3 | 300/3 | 2000/4 | 640/100 | 90/8 |
| $\sigma_z$ [$\mu$m] | 500 | 100 | 80 | 750 | 1000 | 170 |
| Luminosity [$10^{33}$cm$^{-2}$s$^{-1}$] | 2.4 | 5.7 | 3.5 | 12 | 2.6 | 0.7/2.7 |
| $\Upsilon$ | 0.06 | 0.1 | 0.11 | 0.06 | 0.07 | 0.15 |

**Table 1:** *Parameter list of design studies for 500 GeV $e^+e^-$ linear colliders; excerpt from a compilation of Ref.[6].*

By illuminating the incoming electron and positron bunches by laser light, hard Compton back–scattering of the laser photons can be exploited to transform $e^+e^-$ colliders into $e\gamma$ or $\gamma\gamma$ colliders [7]. With the overall luminosity comparable to the original $e^+e^-$ luminosity, the $e\gamma$ spectrum is strongly peaked at about 90% of the total $e^+e^-$ energy. The distribution of the $\gamma\gamma$ invariant energies is broader, yet it can be enhanced strongly near 80% of the total $e^+e^-$ energy by using polarized beams. There is a broad spectrum of physics problems which can be addressed at $e\gamma$ and $\gamma\gamma$ colliders which has recently been reviewed comprehensively [8]. Some specific problems, like Majorana neutrino physics [9], can be studied better in $e^-e^-$ collisions than $e^+e^-$ collisions; this option deserves further studies in the future.

# 2. Top Quark Physics

Top quarks are the heaviest matter particles in the 3–family Standard Model. Introduced to allow for $\mathcal{CP}$ violation in the left–handed charged current sector, strong indirect evidence for the existence of top quarks had been accumulated quite early, based on the $\mathcal{SM}$ gauge symmetry pattern. Deviations from the doublet/singlet pattern of the first two families in the third family would lead to a breaking of the GIM mechanism and thus induce FCNC decays of $B$ mesons at a level several orders above the observed bounds. The isospin quantum numbers of the $b$ quarks can be measured directly through the $Z$–decay width and the forward–backward asymmetry of $b$ quarks in $e^+e^-$ annihilation, the result $I_3^t(b)_{exp} = -0.494 \pm 0.012 \rightarrow -1/2$ demanding the existence of an isospin partner that carries the quantum numbers of the top quark [10].

The top mass enters the $\rho$ parameter, the relative strength between NC and CC processes, quadratically through radiative corrections. Within the framework of the Standard Model, the electroweak high–precision measurements allow us to estimate the value of the top mass [11],

$$m_t = 162^{+16+18}_{-17-21}\ \text{GeV}$$

Top candidate events have been reported by the Tevatron experiments [12], corresponding to a lower limit of the top mass of $\sim 113$ GeV. Final state topologies would be compatible with a top mass of $\sim 152$ GeV, yet within very large errors. If all these candidate events were background events, the lower limit of the top mass would rise to about 160 GeV.

## 2.1 Profile of the Top Quark

For a top mass larger than the $W$ mass the channel

$$t \rightarrow b + W^+$$

is the dominant $\mathcal{SM}$ decay mode. The top quark width grows rapidly, Fig. 1, from small values above the $W$ decay threshold to $\mathcal{O}(1$ GeV) in the mass range $m_t \sim 150$ GeV: $\Gamma(t \rightarrow bW^+) \simeq 175$ MeV $\cdot\, [m_t/m_W]^3$ [13]. The rapid growth is expected from the equivalence theorem since the longitudinal $W$ component, dominating for large $t$ masses, can be identified with the charged Goldstone boson the coupling of which grows with the $t$ mass. The width of the top quark is known to one–loop QCD and



electroweak corrections [14]. The QCD corrections vary slowly from $-8\%$ down to $-10\%$ for top masses above 100 GeV; the electroweak corrections turn out to be small, $\approx +2\%$ for a Higgs mass of $\sim 100$ GeV, and nearly independent of the top mass.

The measurement of the top quark width is very difficult. Three methods have been discussed in the literature. (i) The width of the remnant $1S$ toponium state is given by twice the top width; the smearing due to beamstrahlung however sets stringent limits to the accuracy of this method [15]. (ii) The angular distribution of soft gluons is affected by the non–zero width of the top quark since the finite lifetime leads to a suppression of late infrared and collinear gluon radiation [16]. The sensitivity of the spectra to $\Gamma_t$ however is very low. (iii) A promising method appears to be the analysis of the forward–backward asymmetry of $t$ quarks near the $e^+e^-$ production threshold which may provide an accuracy of 10% [17].

Non–standard top decays could occur in supersymmetric extensions of the Standard Model, top decays into charged Higgs bosons and/or top decays to stop particles,

$$t \rightarrow b + H^+ \quad \textit{and} \quad t \rightarrow \tilde{t} + \tilde{\chi}_1^o$$

if $H^+$ and $\tilde{t}$ are lighter than the top quark. If kinematically allowed, branching ratios of order 10% are expected in both cases [18]. Since the $\mathcal{SUSY}$ parameter space is multi–dimensional, phenomenological constraints on the mass spectrum and the couplings are rather weak beyond the direct limits obtained from $Z$ decays. However, embedding the low–energy minimal $\mathcal{SUSY}$ model into a supergravity motivated grand unified theory and demanding radiative breaking of the electroweak symmetry in this framework, stringent constraints can be derived from the non–observation of supersymmetric particles at LEP and at the Tevatron. They are tightened, Fig. 2, if constraints from photonic $B$ decays are taken into account, mediated by pengiun diagrams to which charged Higgs bosons [19] but also charginos and other $\mathcal{SUSY}$ states, all channels interfering destructively, can contribute [20]. Besides, FCNC decays like $t \rightarrow ch^0$, negligible in the $\mathcal{SM}$, may be enhanced to a detectable level in non-standard Higgs sectors [21].

## 2.2 Static Top Parameters

The main production mechanism for top quarks in $e^+e^-$ collisions is the annihilation channel [22], Fig. 3,

$$e^+e^- \xrightarrow{\gamma,Z} t\bar{t} \rightarrow (bW^+)(\bar{b}W^-)$$

From the subsequent decays $W^\pm \rightarrow f\bar{f}'$ the helicities of the $W$ bosons can be determined so that detailed analyses of the production and decay mechanisms are possible. Because of the large $t$ mass, deviations from the Standard Model may manifest

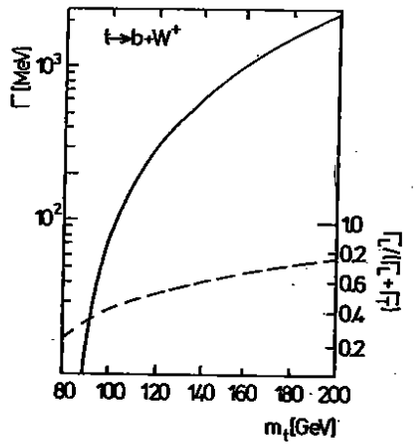


**Fig. 1:** *The top decay width $\Gamma_t$ in the Standard Model, Ref.[13]. The degree of longitudinal W polarization is shown in the insert.*

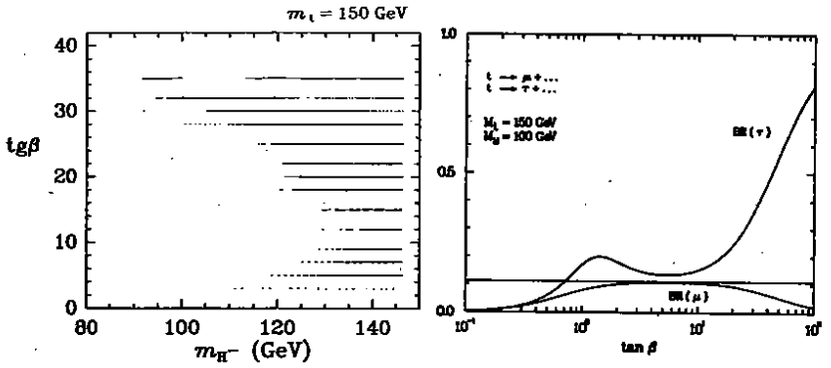


**Fig. 2:** *(a) The allowed range of $[M_{H^+}, \mathrm{tg}\beta]$ values, constrained by the present non-observation of SUSY particles, in GUT models with radiative electroweak symmetry breaking, Ref.[20]. (b) The breaking of $\tau$ vs. $e, \mu$ universality in $t \to bH^+ \to l^+$ decays.*



themselves first in the top quark sector. Examples in which the large $t$ mass is crucial, are provided by multi–Higgs doublet models, models of dynamical symmetry breaking and compositeness. These effects can globally be described by form factors, parametrizing the electroweak ($t\bar{t}$) production current and the weak ($tb$) decay current. As a result of the short lifetime of the $t$ quark, the $t$ quark can be treated as a free particle so that the spin information is not diluted by fragmentation effects. While the general helicity analysis can be found in the literature [23], we shall focus here on a few physically interesting examples.

Magnetic dipole moments of the top quark

If the electrons in $e^+e^- \to t\bar{t}$ are left–handedly polarized, the top quarks are produced preferentially as left–handed particles in the forward direction while only a small fraction is produced as right–handed particles in the backward direction [24]. As a consequence of the $\mathcal{SM}$ prediction, the backward direction is most sensitive to small anomalous magnetic moments of the top quarks. It is apparent from Fig. 4 that the anomalous magnetic moments can be bounded to a few percent by measuring the angular dependence of the $t$ quark cross section.

Electric dipole moments of the top quark

Electric dipole moments are generated by $\mathcal{CP}$–non invariant interactions. Non–zero values of these moments can be signalled by non–vanishing expectation values of $\mathcal{CP}$ odd momentum tensors such as $T_{ij} = (q_+ - q_-)_i(q_+ \times q_-)_j$ with $q_\pm$ being the unit momentum vectors of the $W$–decay leptons. Sensitivity limits to $\gamma, Z$ electric dipole moments are listed in the following table [25] for a top mass of 150 GeV and an integrated luminosity of $\int \mathcal{L} = 10\ \mathrm{fb}^{-1}$:

| $\sqrt{s}$ | $d^{\gamma,Z}$ |
|---|---|
| 300 GeV | $< 7.0 \times 10^{-18}$ e cm |
| 500 GeV | $< 2.8 \times 10^{-18}$ e cm |

Other correlations and energy asymmetries can be defined that are sensitive to $\mathcal{CP}$ violation in the decay current.

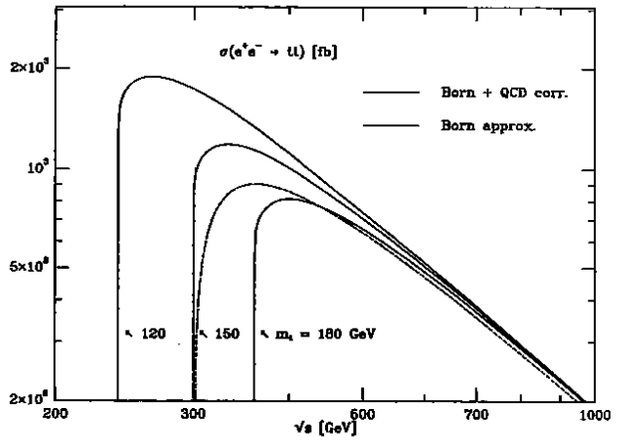


**Fig. 3**: *The cross section $\sigma(e^+e^- \to t\bar{t})$ [including QCD corrections] for three representative values of the top mass.*

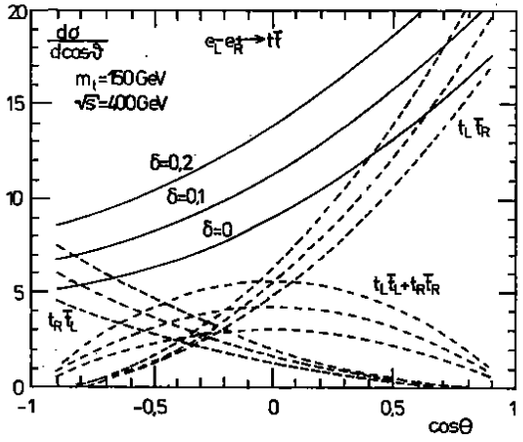


**Fig. 4**: *Angular distributions of the $t$ production cross sections for fixed $t$ and $\bar{t}$ helicities in polarized $e^-_L e^+_R$ annihilation. The parameter $\delta$ measures the anomalous magnetic $(\gamma, Z)$ dipole moment of the top quark. From Ref.[24].*



Chirality of the $(tb)$ decay current

The precise determination of the weak isospin quantum numbers does not allow for large deviations of the $(tb)$ decay current from the left-handed $SM$ prescription. Nevertheless, since $V+A$ admixtures may grow with the masses of the quarks involved [through mixing with heavy mirror quarks, for instance], it is necessary to check the chirality of the decay current directly. The $l^+$ energy distribution in the semileptonic decay chain $t \to W^+ \to l^+$ depends on the chirality of the current. Any deviation from the standard $V-A$ current would lead to a stiffening of the spectrum and, in particular, to a non-zero value at the upper end-point of the energy distribution. A sensitivity to a $V+A$ admixture of 5% can be reached experimentally [26].

## 2.3 The Threshold Region

Quark–antiquark production near the threshold in $e^+e^-$ collisions is of exceptional interest. The long time during which the particles stay close together, allows the strong interactions to build up rich structures of bound states and resonances. This picture applies to top quarks up to the mass range of $\sim 130$ GeV. Beyond this value, the rapid top decay changes the picture quite dramatically: The decay time of the states becomes shorter than the revolution time of the constituents so that toponium resonances cannot be formed any more [13,27]. For a while, remnants of the $1S$ state lead to a peak in the excitation curve, yet it disappears gradually for $t$ masses up to 180 GeV. Nevertheless, across this range the resonance remnants induce a steep rise of the cross section near the threshold.

Since the rapid $t$ decay restricts the interaction region to small distances, the excitation curve can be predicted in perturbative QCD [28,29], based essentially on the Coulombic interquark potential $V(R) = -4/3 \cdot \alpha_s(R)/R$. The cross section is built-up by the superposition of all $nS$ states; this sum can conveniently be performed by using Green's function techniques. The form and the height of the excitation curve are sensitive to the mass of the top quark and the value of the strong coupling constant, Fig. 5. Since an increase of the coupling constant [which lowers the energy levels] can be compensated by a rising top quark mass, the measurement errors of the two parameters are strongly correlated.

This problem can be solved by measuring the momentum spectrum of the top quarks [30] which is determined by the Fourier transform of the wave functions of the overlapping toponium resonances. Since the quarks are confined by the QCD potential, they will have average momenta of order $\langle p \rangle \sim \alpha_s m_t$, corresponding to about 15 GeV. With the product $\alpha_s m_t$ fixed, the two parameters are not positively

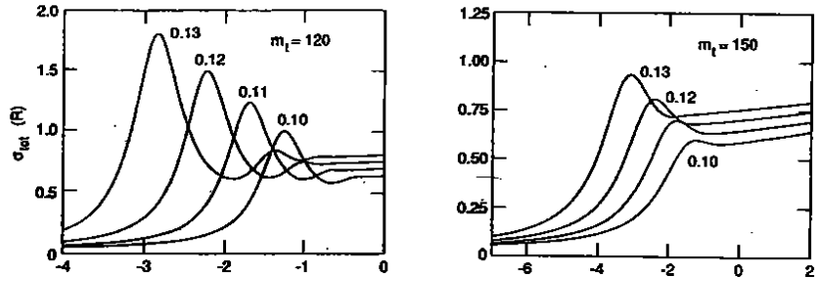


**Fig. 5: (a)** *Excitation curves for t quarks near the threshold for two representative top mass values. The labels at the curves denote the $\alpha_s$ value at the Z mass. From Ref.[29].*

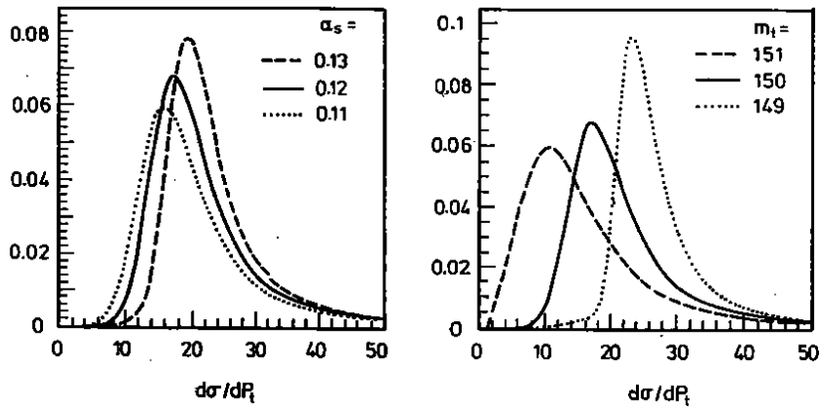


**Fig. 5: (b)** *Momentum distribution of the top quark near the threshold and sensitivity to $m_t$ and $\alpha_s$. From Ref.[31].*



correlated any more so that this measurement is orthogonal to the analysis of the excitation curve.

Detailed experimental simulations predict the following sensitivity to the top mass and the strong coupling constant when combining the two methods [32]:

| $m_t$ [GeV] | $\delta m_t$ [MeV] | $\delta\alpha_s$ |
|---|---|---|
| 120 | 130 | 0.005 |
| 150 | 300 | 0.006 |
| 180 | 520 | 0.009 |

At proton colliders a sensitivity of about 3 GeV can be reached by reconstructing top quarks from jet and lepton final states. Thus, $e^+e^-$ colliders improve the measurement of the top quark mass by about an order of magnitude.

# 3. Electroweak Gauge Bosons

## 3.1 $W$, $Z$ Bosons in the Standard Model

The fundamental electroweak and strong forces appear to be of gauge theoretical origin. This is one of the outstanding results of theoretical and experimental analyses in the past three decades. While the non–abelian gauge theoretical nature of QCD has been successfully demonstrated by evaluating the distribution of hadronic jets in $Z$ decays, only indirect evidence has been accumulated so far for the electroweak $W^\pm$, $Z$, $\gamma$ sector, based on loop corrections to electroweak low–energy parameters and $Z$ observables. HERA, LEP200 and the Tevatron can shed light, for the first time directly, on the triple couplings of the electroweak gauge bosons as prescribed by the gauge symmetries. Since deviations from the gauge symmetry prescriptions manifest themselves in experimental observables with coefficients $(\beta\gamma)^2$, only the very high energies of future $pp$ end $e^+e^-$ colliders will allow, however, stringent direct

tests of the self–couplings of the electroweak gauge bosons. The high efficiency for reconstructing $W$, $Z$ bosons in the clean environment of $e^+e^-$ collisions makes a 500 GeV collider superior even to the SSC in this context.

The gauge symmetries of the Standard Model determine the form and the strength of the self–interactions of the electroweak bosons, triple couplings $WW\gamma, WWZ$ and quartic couplings. Deviations from the gauge symmetry form of these vertices, as well as novel couplings like $ZZZ$ in addition to the canonical $\mathcal{SM}$ couplings, could be expected in more general scenarios. In models with composite $W, Z$ bosons for instance, corrections could alter the vertices to order $[M_W/\Lambda_{\rm comp}]^j$ and induce new types of couplings [33,34]. Other examples are provided by models in which the $W, Z$ bosons are generated dynamically or interact strongly with each other.

While the experimental analyses of the self–couplings of the electroweak bosons can be carried out at collider energies of 500 GeV with high accuracy, $WW$ scattering can only be studied at energies in the TeV range. This is a very important process to be investigated if light Higgs particles do not exist and $W$ bosons become strongly interacting particles at high energies.

The triple gauge boson couplings

The couplings $W^+W^-\gamma$ and $W^+W^-Z$ are in general described by seven parameters each. Assuming $\mathcal{C}, \mathcal{P}$ and $\mathcal{T}$ invariance in the pure electroweak boson sector, the number of parameters can be reduced to three [35],

$$\mathcal{L}_\gamma/g_\gamma = ig_\gamma^1 W^*_{\mu\nu}W_\mu A_\nu + \text{h.c.} \; + \; i\kappa_\gamma W^*_\mu W_\nu F_{\mu\nu} \; + \; i\frac{\lambda_\gamma}{M_W^2}W^*_{\rho\mu}W_{\mu\nu}F_{\nu\rho}$$
$$\mathcal{L}_Z/g_Z = [\gamma \to Z]$$

which may be identified with the $\gamma, Z$ charges of the $W$ bosons and the related magnetic dipole moments and electric quadrupole moments,

$$\mu_\gamma = \frac{e}{2M_W}(1+\kappa_\gamma+\lambda_\gamma) \quad \text{and} \quad [\gamma \to Z]$$
$$Q_\gamma = -\frac{e}{M_W^2}(\kappa_\gamma - \lambda_\gamma) \qquad \text{and} \quad [\gamma \to Z]$$

The gauge symmetries of the $\mathcal{SM}$ demand $\kappa = 1$ and $\lambda = 0$, i.e. $\mu_\gamma = e/M_W$ and $Q_\gamma = -e/M_W^2$ etc. The magnetic dipole and the electric quadrupole moments can be measured *directly* through the production of electroweak boson $W\gamma$ and $WZ$ pairs at $p\bar{p}/pp$ colliders and $WW$ pairs at $e^+e^-$ [and $\gamma\gamma$] colliders.



(a) *Agnostic approach*

Couplings among weakly interacting vector bosons must be of non–abelian gauge structure in order to be compatible with the requirements of unitarity at asymptotic energies. However, if new physical structures appear at a finite scale $\Lambda$, associated for instance with a non–zero size of the vector bosons, the triple and quartic couplings will be modified at order $[M_W/\Lambda]^j$. For a minimum scale $\Lambda \sim 1$ TeV and $j = 2$, corrections of a few percent could plausibly be expected. Detailed experimental analyses [see Refs. [1-3]] have been carried out for the reaction

$$e^+e^- \longrightarrow W^+W^- \to (l\nu_e)(q\bar{q}')$$

demonstrating that bounds of order

$$\Delta\kappa_j, \lambda_j \leq \pm 0.02$$

can be reached at collider energies of 500 GeV. For $\kappa$, the bound obtained at the $e^+e^-$ collider is significantly better than the bound at proton colliders, Fig. 6. The bounds improve to $\sim 0.002$ if the $e^+e^-$ energy is raised to 1.5 TeV. Note that in both cases the range being probed extends beyond the energy scale accessible directly — not much though.

(b) *Orthodox approach*

It is a theoretically attractive concept to assume that any deviations from the Standard Model due to new physics may phenomenologically manifest themselves in SU(3) × SU(2) × U(1) gauge invariant $\mathcal{SM}$ singlet operators [37]. To the extent that the operators affect the gauge boson propagators, they are stringently constraint by the high–precision low–energy data from $Z$ boson physics etc. These operators affect the triple boson couplings at a level of less than $10^{-3}$. However, there are sets of operators which are only weakly constrained by propagator effects so that deviations from the Standard Model of order $10^{-2}$ cannot be excluded [38]. Classifying these operators as

$$\delta\mathcal{L} = \frac{f_{WWW}}{\Lambda^2}\mathcal{O}_{WWW} + \frac{f_W}{\Lambda^2}\mathcal{O}_W + \frac{f_B}{\Lambda^2}\mathcal{O}_B$$

with $\mathcal{O}_{WWW} = \text{tr}\,[W^3]$ and $\mathcal{O}_{W/B} = (D\phi)^*(W/B)(D\phi)$, the five free triple boson couplings can be expressed through three parameters,

$$\Delta g_1^Z = \frac{M_Z^2}{2\Lambda^2}f_W \qquad \Delta\kappa_\gamma = \frac{M_Z^2}{2\Lambda^2}[f_W - s_W^2(f_B+f_W)]$$
$$\lambda_Z = \lambda_\gamma = \frac{3M_W^2 g_W^2}{2\Lambda^2}f_{WWW} \qquad \Delta\kappa_Z = \frac{M_Z^2}{2\Lambda^2}c_W^2(f_B+f_W)$$

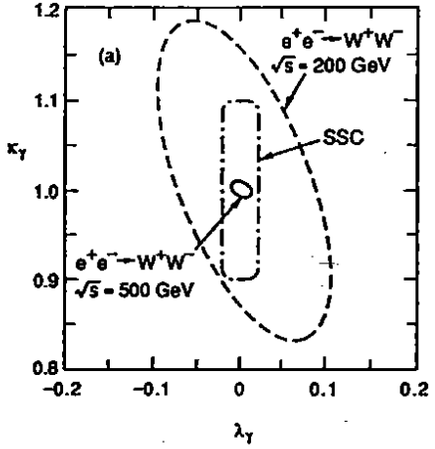


**Fig. 6**: *Projections onto the $(\kappa_\gamma, \lambda_\gamma)$ plane of the 95% CL joint probability ellipsoid. SM values are assumed for $(\kappa_Z, \lambda_Z)$ in the $e^+e^-$ analysis; this assumption can be avoided at the expense of slightly larger integrated luminosities. Luminosities of $\int \mathcal{L} = 10\ fb^{-1}$ at $\sqrt{s} = 500\ GeV$, $\int \mathcal{L} = 1.3\ fb^{-1}$ at $\sqrt{s} = 200\ GeV$ and $\int \mathcal{L} = 10\ fb^{-1}$ at the SSC are assumed. From Ref.[36].*

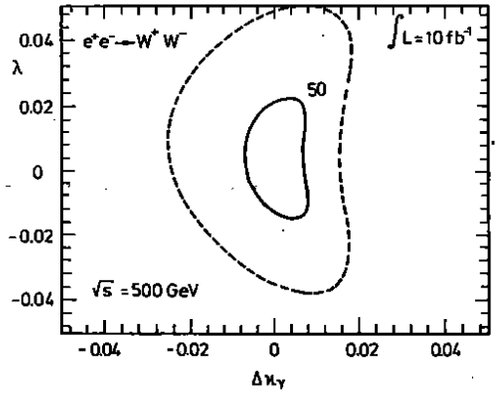


**Fig. 7**: *Two-parameter fit to $(\kappa_\gamma, \kappa_z)$ in the orthodox approach in which any contribution to the self-couplings of the electroweak bosons in addition to the Standard Model is assumed to be due to $SU(3) \times SU(2) \times U(1)$ singlet operators. From Ref.[39].*



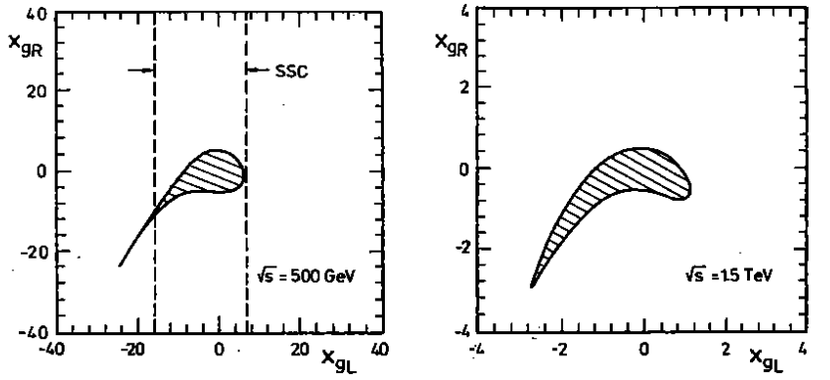


**Fig. 8**: *Bounds on the chiral parameters $x_{9L}$ and $x_{9R}$ that can be reached at $e^+e^-$ collider energies of 500 GeV and 1.5 TeV. From Ref.[41].*

Two–parameter fits, Fig. 7, give very stringent bounds on the boson couplings for 500 GeV and $\int \mathcal{L} = 50\ fb^{-1}$:

$$\Delta\kappa_\gamma, \Delta\kappa_Z \leq \pm 0.006, \pm 0.006$$
$$\Delta\kappa_\gamma, \lambda \leq \pm 0.008, \pm 0.02$$

### (c) *Calvinistic approach*

In theories without light Higgs particles, the electroweak gauge bosons interact strongly with each other above $\sim$ 1 TeV. Such a scenario can be described by a non–linear realization of the symmetry in a chiral Lagrangian formalism [40],

$$\delta\mathcal{L} = i\frac{x_{9L}}{16\pi^2}\mathrm{tr}\,[g_W W_{\mu\nu} D_\mu U^+ D_\nu U] - i\frac{x'_{9R}}{16\pi^2}\mathrm{tr}\,[g'_W B_{\mu\nu} D_\mu U^+ D_\nu U]$$
$$+ \frac{x_{10}}{16\pi^2}\mathrm{tr}\,[U^+ g'_W B_{\mu\nu} U g_W W_{\mu\nu}], \qquad U = exp\, i\,\pi/v$$

For $x_i \sim \mathcal{O}(1)$ the anomalous moments acquire values of $\mathcal{O}(10^{-2})$. Experimental analyses have shown, Fig. 8, that for 500 GeV the parameter $x_9$ can be constraint to values less than 5 to 10. However, energies of $\sim$ 1.5 TeV are needed to suppress it to a value less than unity.

Strongly interacting $W$, $Z$ bosons

If the scenario in which $W$, $Z$, Higgs bosons are weakly interacting up to the GUT scale [requiring a Higgs mass of less than 200 GeV] is not realized in Nature, the next possible scenario is a strongly interacting $W$, $Z$ sector. Without a light Higgs of less than about 1 TeV, the electroweak bosons must become strongly interacting at energies of about 1.2 TeV to fulfill the requirements of unitarity for the $WW$ scattering amplitudes [42]. New strong interactions may build up the longitudinal degrees of freedom of the massive vector bosons in technicolor theories, for instance. In such a case, new types of resonances could be realized in the $\mathcal{O}$(1 TeV) energy range; however, the formation of resonances in $W_LW_L$ scattering could also be delayed until several TeV.

In the strongly interacting vector boson scenario, $W_LW_L$ scattering must be studied at energies of order 1 TeV which require the highest energies possible in the 1.5 to 2 TeV range at $e^+e^-$ colliders. (Quasi)elastic $WW$ scattering can be investigated by using $W$ bosons radiated off the $e^\pm$ beams, or by exploiting final state interactions in $e^+e^-$ annihilation to $W$ pairs. All possible (isospin, angular momentum) combinations in $WW$ scattering amplitudes $a_{IJ}$ can be realized in the first process. The cross

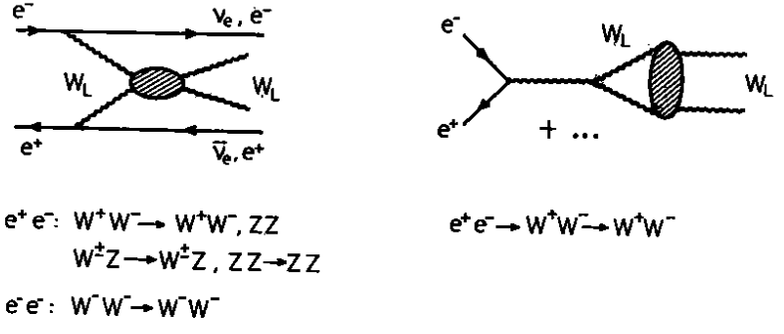


sections however are small as long as no resonances are formed. A complementary method is the rescattering method in $e^+e^-$ annihilation to $W^+W^-$ pairs in which the $(I,J)=(1,1)$ $WW$ scattering phase shift enters through the Omnès factor,

$$a_{11} = a_{11}^{(0)} \exp\left[\frac{s}{\pi}\int \frac{ds'\delta_{11}(s')}{s'(s'-s)}\right]$$

Building up the vector boson masses through spontaneous breaking of the electroweak symmetries, the longitudinal degrees of freedom of the vector bosons can be



identified at high energies with the Goldstone bosons associated with the spontaneous symmetry breaking. In analogy to the $\pi\pi$ low-energy theorems, the first term in the energy expansion of the $WW$ scattering amplitudes is determined independently of dynamical details, $a_{00}=+6, a_{11}=+1, a_{20}=-2$ in units of $1/96\pi v^2$. The attractive $I=0$ and 1 channels may form Higgs and $\rho$-type resonances at high energies. While "$H,p$" resonances would alter the scattering amplitudes dramatically compared with the predictions in a light–Higgs scenario, the low-energy theorems nevertheless affect the cross sections significantly, too. For $\sqrt{s}=1.5$ TeV and $\sqrt{s_{WW}}>500$ GeV, the predictions for the scattering cross sections in the weak scenario with a light Higgs mass are confronted with the strong scenario in the following table [43]:

| $\sigma$ [fb] | Weak Scenario | Strong Scenario |
|---|---|---|
| $e^+e^- \to \bar{\nu}\nu WW$ | 0.45 | 0.68 |
| $e^+e^- \to \bar{\nu}\nu ZZ$ | 0.37 | 0.74 |

Similar effects would also be observed in $\sigma(e^+e^- \to W^+W^-)$. $(I,J)=(1,1)$ resonance effects would be noticeable at $\sqrt{s}=1$ TeV up to resonance masses of about 5 TeV in angular distributions of the $W$ decay final states [44].

## 3.2 Extended Gauge Theories

Despite its tremendous success in describing the experimental data within the range of energies available today, the Standard Model based on the gauge symmetry SU(3) × SU(2) × U(1) is widely believed not to be the *ultima ratio*. Besides the fact that it has too many parameters which are merely incorporated by hand, the $\mathcal{SM}$ does not unify the electroweak and strong forces in a satisfactory way since the coupling constants of these interactions are different and appear to be independent. Therefore one would expect that a more fundamental theory exists which describes the three forces within the context of a single gauge group and hence, with only one coupling constant. This grand unified theory will be based on a gauge group containing SU(3) × SU(2) × U(1) as a subgroup and it will be reduced to this symmetry at low energies.

Two predictions of grand unified theories may have dramatic phenomenological consequences in the energy range of a few hundred GeV [45]:

(i) The unifying symmetry group must be spontaneously broken at the unification scale, $\Lambda_{\rm GUT} > 10^{15}$ GeV in order to be compatible with the experimental bounds on

the proton lifetime. However, it is possible that the breaking to the $\mathcal{SM}$ group occurs in several steps and that some subgroups remain unbroken down to a scale of order 1 TeV. In this case the surviving group factors allow for new gauge bosons with masses not far from the scale of electroweak symmetry breaking. Besides SU(5), two other unifying groups have received much attention in recent years. In SO(10) three new gauge bosons $W_R^{\pm}, Z_R$ are predicted, while in E(6) a light neutral $Z'$ may exist in the TeV range.

The virtual effects of a new $Z'$ associated with the most general effective theories which arise from breaking E(6), $SU(3) \times SU(2) \times U(1) \times U(1)_{Y'}$, and $SO(10), SU(2)_L \times SU(2)_R \times U(1)$, have been investigated in Ref. [46,47]. Assuming that the $Z'$ is heavier than the c.m. energy, its propagator effects on various observables of the process $e^+e^- \to f\bar{f}$ have been studied. The effects of the new $Z'$ can be probed between 1.5 and 3 TeV at a 500 GeV collider, Fig. 9a, while they may be produced directly up to $\sim 5$ TeV at hadron colliders. However, the $e^+e^-$ collider can help to identify the physical nature of the new boson, Fig. 9b. At a 1.5 TeV collider, the mass window can be extended up to 4.5 .... 9 TeV, far beyond the reach of proton colliders. Additional information can be obtained from $W$-pair production [48].

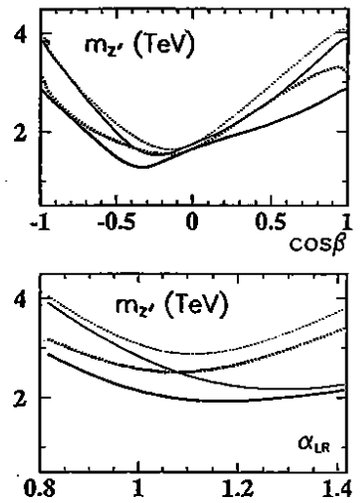


**Fig. 9: (a)** *$Z'$ mass limits in models with an extra U(1) and left–right models. Solid (dotted) lines: without (with) polarization.*

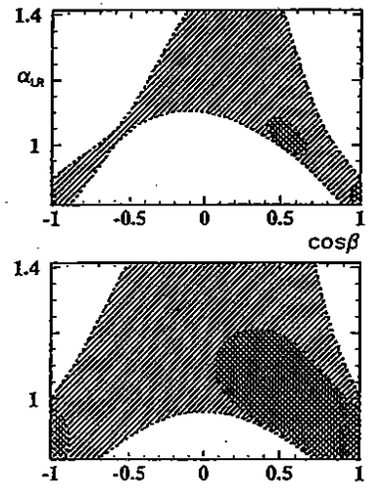


**Fig. 9: (b)** *Distinction between models with an extra U(1) and left–right models. Top (bottom): $M_{Z'}$ =1.5 (2) TeV. Ref.[46].*



(ii) The grand unified groups incorporate extended fermion representations in which a complete generation of $\mathcal{SM}$ quarks and leptons can be naturally embedded. These representations accommodate a variety of additional new fermions. It is conceivable that the new fermions [if they are protected by symmetries, for instance] acquire masses not much larger than the Fermi scale. This is very likely, and even necessary if the predicted new gauge bosons are relatively light. SO(10) is the simplest group in which the 15 Weyl spinors of each $\mathcal{SM}$ generation of fermions can be embedded into a single multiplet. This representation has dimension **16** and contains a right–handed neutrino. The group E(6) contains SU(5) and SO(10) as subgroups. In E(6), each quark–lepton generation lies in a representation of dimension **27**. To complete this representation, twelve new fields are needed in addition to the $\mathcal{SM}$ fermion fields. For each family one has two additional isodoublets of leptons, two isosinglet neutrinos and an isosinglet quark with charge $-1/3$.

If the new particles have non–zero electromagnetic and weak charges, they can be pair produced if their masses are smaller than the beam energy of the $e^+e^-$ collider. In general, the processes are built–up by a superposition of $\gamma$ and $Z$ exchange, but additional contributions could come from the extra neutral bosons if their masses are not much larger than the c.m. energy [49]. At a 500 GeV collider, the cross sections are fairly large, apart from phase space suppression factors, of the order of the point–like QED cross section $\sigma(e^+e^- \to F\overline{F}) \sim \sigma_0 \simeq 400$ fb. This leads to samples of several thousands of events. The large number of events allows to probe masses up to the kinematical limit of 250 GeV. Fermion mixing, if large enough, leads to an additional production mechanism for the new fermions: single production in association with their light partners. In this case, masses very close to the total energy of the $e^+e^-$ collider can be reached. For the second and third generation of leptons [if inter–generational mixing is neglected] and for quarks, the process proceeds only through $s$–channel $Z$ exchange and leads to relatively small cross sections. But in the case of the first generation leptons, additional $t$–channel exchanges [$W$ exchange for neutral leptons and $Z$ exchange for charged leptons] are present, increasing the cross sections eventually by several orders of magnitude to a level of $10^2$ to $10^3 fb$.

# 4. Higgs Bosons

The Higgs mechanism is a cornerstone in the electroweak sector of the Standard Model. The fundamental particles, leptons, quarks and weak gauge bosons, acquire their masses through the interaction with a scalar field. To accommodate the well–established electromagnetic and weak phenomena, the Higgs mechanism requires the existence of at least one weak iso–doublet scalar field. After absorbing three Goldstone modes to build up the longitudinal polarization states of the $W^{\pm}, Z$ bosons, one degree of freedom is left–over, corresponding to a real scalar particle. The discovery of this Higgs particle is the *experimentum crucis* for the standard formulation of the electroweak interactions.

The only unknown parameter in the $\mathcal{SM}$ Higgs sector is the mass of the Higgs particle. Interesting constraints on the mass can, however, be derived from assumptions on the energy range within which the model be valid before perturbation theory breaks down at a scale $\Lambda$ and new dynamical phenomena would emerge [50]. The strength of the Higgs self–interaction is determined by the Higgs mass itself at the scale $M_H$. Increasing the scale, the quartic self–coupling of the Higgs field grows logarithmically with the energy scale, similarly to the electromagnetic coupling in QED. If the Higgs mass is small, the energy cut–off $\Lambda$ is large at which the coupling grows beyond any bound; conversely, if the Higgs mass is large, the cut–off $\Lambda$ is small. The condition $M_H < \Lambda$ sets an upper limit on the Higgs mass in the Standard Model. Analyses of the non–perturbative regime near the cut–off lead to an estimate of about 630 GeV for the upper limit of $M_H$. However, if the Higgs mass is less than 180 to 200 GeV, the Standard Model can be extended up to the GUT scale $\Lambda_{\rm GUT} \sim 10^{15}$ GeV, with the particles remaining weakly interacting. The hypothesis that interactions between $W, Z$ bosons and Higgs particles remain weak up to the GUT scale plays a key rôle in explaining the experimental value of the electroweak mixing parameter $\sin^2\theta_W$. Based on the $\mathcal{SM}$ particle spectrum, the mixing parameter evolves from the symmetry value 3/8 at the GUT scale down to $\sim 0.2$ at $\mathcal{O}(100$ GeV). Even though additional degrees of freedom are needed to account for the [small] discrepancy to the experimentally observed value 0.23, the hypothesis that the particle interactions remain weak up to the GUT scale, is nevertheless qualitatively supported by this result. From this assumption and the additional requirement of vacuum stability, upper and lower bounds on the Higgs mass can be derived. Based on these arguments, the Higgs mass could be expected in the window $100 < M_H < 180$ GeV for a top mass value of about 150 GeV.

A large variety of channels can be exploited to search for Higgs particles in the bremsstrahl and fusion processes of $e^+e^-$ colliders [51]. In the bremsstrahl process $e^+e^- \to ZH$, missing–mass techniques can be exploited in events with leptonic $Z$ decays or the Higgs particle may be reconstructed in $H \to b\bar{b}, WW$ directly. The



$WW$ fusion process $e^+e^- \to \bar{\nu}\nu H$ requires the reconstruction of the Higgs particle, while missing–mass techniques can also be used in $ZZ$ fusion.

Once the Higgs boson has been found, it will be very important to explore its properties. This is possible at great detail in the clean environment of $e^+e^-$ colliders. The zero–spin of the Higgs particle is reflected in the angular distribution of the bremsstrahl process which asymptotically must follow the $\sin^2\theta$ law. Of tantamount importance is the measurement of the couplings to gauge bosons and matter particles. The strength of the couplings to $Z$ and $W$ bosons is reflected in the magnitude of the $e^+e^-$ production cross sections. The strength of the couplings to fermions is accessible through the decay branching ratios and Higgs bremsstrahlung off top quarks.

From the preceding discussion we conclude that $e^+e^-$ linear colliders with energies in the range of 300 to 500 GeV are ideal instruments to search for Higgs particles in the intermediate mass range which, *a priori*, may be considered as a very important part in the entire range of possible Higgs mass values.

An even stronger case for linear colliders is made by supersymmetric extensions of the Standard Model. In particular, the Minimal Supersymmetric extension of the Standard Model ($\mathcal{MSSM}$) incorporates a Higgs scenario which, beyond any doubt, can best be explored in $e^+e^-$ colliders. Even though the $\mathcal{MSSM}$ is a specific realization of supersymmetry, some of the key features are expected to be realized in more general $\mathcal{SUSY}$ models too, so that the analysis can be considered as representative for a wide class of models.

The $\mathcal{MSSM}$ requires the existence of two iso–doublets of scalar fields, giving mass separately to up and down–type fermions. Three neutral [$h^0/H^0(\mathcal{CP}=+), A^0(\mathcal{CP}=-)$] and a pair of charged scalar particles [$H^{\pm}$] are introduced by this extension of the Higgs sector. At tree level, the mass of the lightest Higgs boson $h^0$ is smaller than the $Z$ mass. Radiative corrections however, which grow as the fourth power of the top quark mass, can shift the upper bound from $M_Z$ to $\sim 130$ GeV. Beyond $\sim 90$ GeV, Higgs particles are not accessible anymore at LEP200 and higher energies are required to produce these particles. The masses of the heavy neutral and charged Higgs bosons can be expected, with high probability, in the range of the electroweak symmetry breaking scale so that a large part of the mass parameter space can be covered at an $e^+e^-$ collider with an energy of 500 GeV. At hadron colliders the detection of these particles is not guaranteed. Combining all $e^+e^-$ production channels at least the lightest of the neutral Higgs particles must be found at the linear collider. If not, the minimal supersymmetric extension of the Standard Model is ruled out. Furthermore, in a large part of the parameter space *all* the neutral Higgs particles and the charged Higgs particles can be found. The detailed comparison of branching ratios and production cross sections with the predictions of the $\mathcal{MSSM}$ will eventually shed light on the physical basis of the extended Higgs sector.

## 4.1 Higgs in the Standard Model

Decay and production

The profile of the $\mathcal{SM}$ Higgs particle is uniquely determined if the Higgs mass is fixed. For Higgs particles in the intermediate mass range $M_Z \leq M_H \leq 2M_Z$ the main decay modes are decays into $b\bar{b}$ pairs and $WW, ZZ$ pairs with one of the gauge bosons being virtual below the respective threshold. Above the $WW$ threshold, the Higgs particles decay almost exclusively into these channels. Below 140 GeV, the decays $H \to \tau^+\tau^-, c\bar{c}$ and $gg$ are also of significance besides the dominating $b\bar{b}$ channel. By adding up all possible decay channels, we obtain the total Higgs decay width shown in Fig. 10 for $m_t = 150$ GeV. Up to masses of 140 GeV, the Higgs particle is very narrow, $\Gamma(H) \leq 10$ MeV. After opening the [virtual] gauge boson channels, the state becomes rapidly wider, reaching $\sim 1$ GeV at the $ZZ$ threshold. The width cannot be measured directly in the intermediate mass range. Only above $M_H \geq 200$ GeV it becomes wide enough to be resolved experimentally.

The main production mechanisms for Higgs particles in $e^+e^-$ collisions are Higgs bremsstrahlung off the $Z$ boson line

$$e^+e^- \to (Z) \to Z + H$$

and the fusion processes

$$e^+e^- \to \bar{\nu}\nu\,(WW) \to \bar{\nu}\,\nu + H$$
$$e^+e^- \to e^+e^-(ZZ) \to e^+e^- + H$$

with the [virtual] vector bosons radiated off the initial electrons and positrons.

The cross section for the bremsstrahl process and the fusion processes [52–54] are shown in Fig. 11 for 300 and 500 GeV c.m. energy. A rate of $\sim$ 2,000 Higgs particles will be produced for an integrated luminosity of $\int \mathcal{L} = 10$ fb$^{-1}$. With rising energy the bremsstrahl cross section scales $\sim s^{-1}$ while the fusion cross sections increase logarithmically $\sim M_W^{-2} \log s/M_W^2$, becoming dominant above 500 GeV.

The recoiling $Z$ boson in the two–body reaction $e^+e^- \to ZH$ is mono–energetic and the mass can be derived from the energy of the $Z$ boson, $M_H^2 = s - 2\sqrt{s}E_Z + M_Z^2$. Initial state bremsstrahlung and beamstrahlung smear out the peak slightly. $ZZ$ production does not pose a background problem; if $b$ tagging devices are used, even not for Higgs masses close to the $Z$ mass, as shown in Fig. 12. A similarly clear peak can be observed in the fusion process $e^+e^- \to \overline{\nu}\nu H$ by collecting the decay products of the Higgs boson. The dominant background process in this case is the reaction $e^+e^-$ $\to (e^+)\nu_e W^-$, with the final state positron travelling along the beam pipe; however, this background is negligible for Higgs masses above $\sim$ 110 GeV even if experimental resolution effects are taken into account.



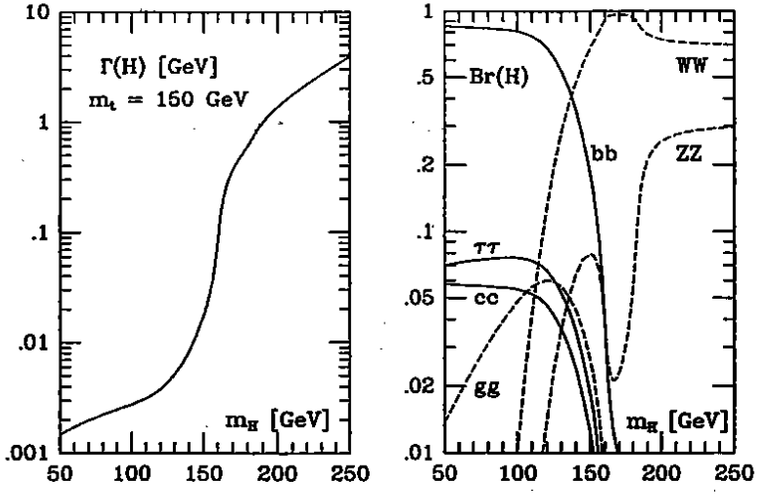


**Fig. 10:** *(a) Decay width and (b) decay branching ratios of the Higgs particle in the Standard Model.*

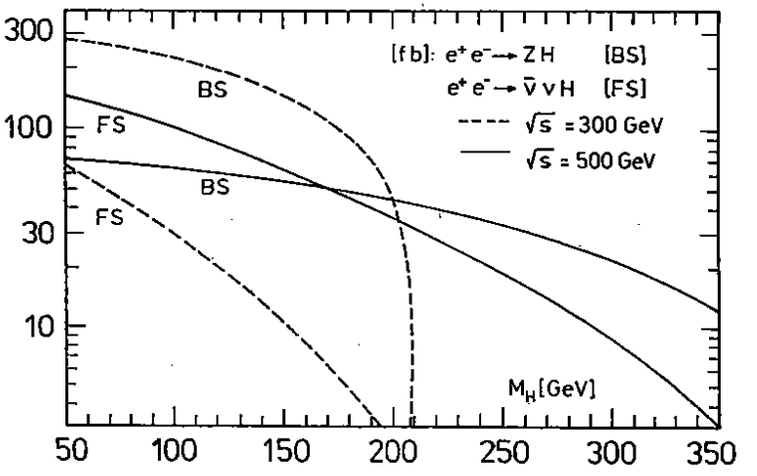


**Fig. 11:** *Production cross sections for Higgs bremsstrahlung and fusion in the Standard Model.*

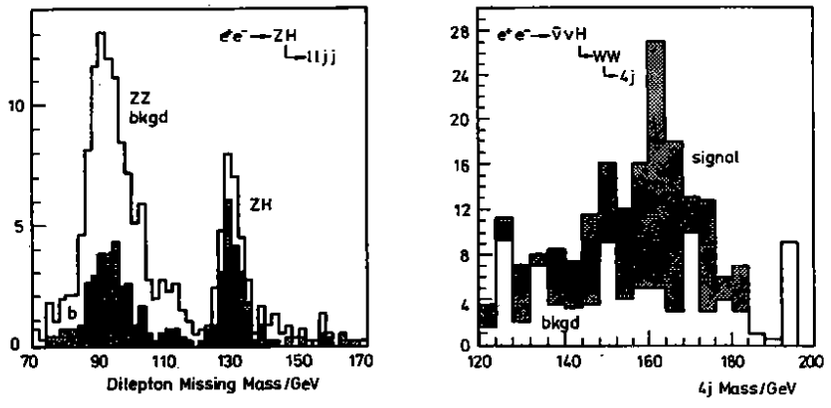


**Fig. 12:** *(a) Missing mass distribution in bremsstrahl production of Higgs bosons; (b) invariant mass distribution of the Higgs decay products in WW fusion. Ref.[55].*

The profile of the $\mathcal{SM}$ Higgs particle

The angular distribution of the $Z/H$ bosons in the bremsstrahl process is sensitive to spin and parity of the Higgs particle [53]. Since the amplitude is given by $\mathcal{A}(0^+) \sim \vec{\varepsilon}_1 \cdot \vec{\varepsilon}_2$, the $Z$ boson is produced in a state of longitudinal polarization at high energies, — in accord with the equivalence theorem. As a result, the angular distribution $d\sigma/d\cos\theta \sim \lambda \sin^2\theta + 8M_Z^2/s$ approaches the spin–zero law $\sin^2\theta$ asymptotically. This may be contrasted with the distribution $\sim 1 + \cos^2\theta$ for negative parity states, following from the transverse polarization amplitude $\mathcal{A}(0^-) \sim \vec{\varepsilon}_1 \times \vec{\varepsilon}_2 \cdot \vec{k}_Z$. It is also characteristically different from the background process $e^+e^- \to ZZ$ which is strongly peaked in the forward/backward direction, Fig. 13.

Since the fundamental particles acquire masses through the interaction with the Higgs field, the scale of the Higgs couplings to fermions and gauge bosons is set by the masses of these particles. It will be mandatory to measure the Higgs couplings to the fundamental particles, which are uniquely predicted by the very nature of the Higgs mechanism. The Higgs couplings to massive gauge bosons can directly be determined from the measurement of the production cross sections with an accuracy of $\pm 3\%$: the $HZZ$ coupling in the bremsstrahl and the $HWW$ coupling in the fusion process. For Higgs couplings to fermions, either loop effects in $H \rightleftharpoons gg, \gamma\gamma$ [mediated by top quarks] must be exploited, or the measurement of branching ratios $H \to b\bar{b}, c\bar{c}, \tau^+\tau^-, gg$ in the lower part of the intermediate mass range. This is exemplified for a Higgs mass of 140 GeV in Fig. 14. A direct way to determine the Yukawa coupling



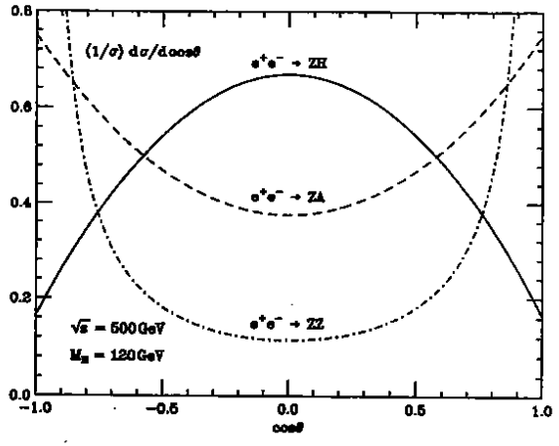


**Fig. 13:** *Angular distribution of the bremsstrahl process $e^+e^- \to ZH$, confronted with pseudoscalar particle production and $ZZ$ background final states [53].*

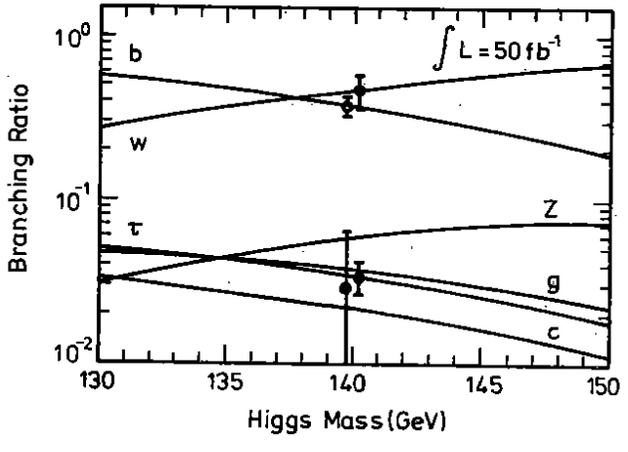


**Fig. 14:** *Measurements of the branching ratios for $\mathcal{SM}$ Higgs decays into $WW, b\bar{b}, \tau^+\tau^-$ and $c\bar{c} + gg$ final states, Ref.[56].*

of the intermediate mass Higgs boson to the top quark in the range $m_H \leq 120$ GeV is provided by the bremsstrahl process $e^+e^- \to t\bar{t}H$ in high energy $e^+e^-$ colliders [57]. For large Higgs masses above the $t\bar{t}$ threshold, the decay channel $H \to t\bar{t}$ increases the cross section of $e^+e^- \to t\bar{t}Z$ through the reaction $e^+e^- \to ZH(\to t\bar{t})$ [58]. Higgs exchange between $t\bar{t}$ quarks affects also the excitation curve near the threshold at a level of a few percent.

## 4.2 $\mathcal{SUSY}$ Higgs Particles

Supersymmetric theories are most appealing extensions of the Standard Model. They provide a theoretical framework in which the problems of hierarchy and naturalness are solved while retaining the Higgs bosons as elementary spin–zero particles. The Minimal Supersymmetric extension of the Standard Model may serve as a useful guideline into this area. Though some of the phenomena will be specific to this minimal version, many of the patterns will also be valid in more general extensions.

The Higgs spectrum in the $\mathcal{MSSM}$ consists of five states, $h, H, A$ and $H^\pm$. Besides the masses, two mixing angles define the properties of the scalar particles and their interactions with gauge bosons and fermions, the ratio of the two vacuum expectation values $\mathrm{tg}\beta = v_2/v_1$ and a mixing angle $\alpha$ in the neutral $\mathcal{CP}$–even sector. Supersymmetry leads to several relations among these parameters and, in fact, only two of them are independent. These relations impose a strong hierarchical structure on the mass spectrum [$M_h < M_Z, M_A < M_H$ and $M_W < M_{H^\pm}$] which however is broken by radiative corrections if the top quark mass is large [59].

The couplings of the various neutral Higgs bosons to fermions and gauge bosons will in general depend on the angles $\alpha$ and $\beta$. The pseudoscalar boson $A$ does not have tree–level couplings to gauge bosons, and its couplings to down (up) type fermions are (inversely) proportional to $\mathrm{tg}\beta$. The couplings depend in general strongly on the input parameters $\mathrm{tg}\beta$ and the masses. The couplings to down (up) type fermions are enhanced (suppressed) compared to the $\mathcal{SM}$ Higgs couplings. If $M_h$ is very close to its upper limit for a given value of $\mathrm{tg}\beta$, the couplings to fermions and gauge bosons are $\mathcal{SM}$ like.

Decay Modes

The lightest neutral Higgs boson will decay mainly into fermion pairs since its mass is smaller than $\sim$ 130 GeV, Fig. 15. This is also the dominant decay mode of the



pseudoscalar boson $A$. For values of $\mathrm{tg}\beta$ larger than unity and for masses less than $\sim$ 140 GeV, the main decay modes of the neutral Higgs bosons are decays into $b\bar{b}$ and $\tau^+\tau^-$ pairs; the branching ratios being always larger than $\sim$ 90% and 8%, respectively. The decays into $c\bar{c}$ pairs and gluons [proceeding through $t$ and $b$ quark loops] are strongly suppressed especially for large $\mathrm{tg}\beta$. For large masses, the top decay channels $H, A \to t\bar{t}$ open up; yet this mode remains suppressed for large $\mathrm{tg}\beta$. For large $\mathrm{tg}\beta$, the neutral Higgs bosons decay almost universally into $b\bar{b}$ and $\tau^+\tau^-$ pairs. If the mass is high enough, the heavy $\mathcal{CP}$–even Higgs boson $H$ can in principle decay into weak gauge bosons $H \to WW, ZZ$. Since the partial widths are proportional to $\cos^2(\beta-\alpha)$, they are strongly suppressed and the gold–plated $ZZ$ signal of the heavy $\mathcal{SM}$ Higgs boson is lost in the supersymmetric extension. The heavy neutral Higgs boson $H$ can also decay into two lighter Higgs bosons. These modes, however, are restricted to very small domains in the parameter space.

Other possible channels are decays into supersymmetric particles. While sfermions are likely too heavy to affect Higgs decays in the mass range considered here, Higgs boson decays into charginos and neutralinos could eventually be important since the masses of some of these particles are expected to be of order $M_Z$. These new channels are kinematically accessible at least for the heavy Higgs bosons $H, A$ and $H^\pm$; in fact, the branching fractions can be very large and they can even be dominant in some regions of the $\mathcal{MSSM}$ parameter space [60]. Decays of $h$ into the lightest neutralinos ($LSP$) are also important, exceeding 50% in some corners of the $\mathcal{SUSY}$ parameter space. These decays strongly affect experimental search techniques. In particular, neutral Higgs decays into the $LSP$ which would be invisible, could jeopardize the search for the Higgs particles at hadron colliders where these decay modes are very difficult to detect. At $e^+e^-$ colliders however, missing mass techniques allow us to isolate these events easily, at least for the $\mathcal{CP}$–even Higgs bosons which can be produced in association with the $Z$ boson. [Other invisible decay modes of Higgs bosons are summarized in Ref.[61].]

The charged Higgs particles decay into fermions but also, if allowed kinematically, into the lightest neutral Higgs and a $W$ boson. Below the $tb$ and $Wh$ thresholds, the charged Higgs particles will decay mostly into $\tau\nu_\tau$ and $c\bar{s}$ pairs, the former being dominant for $\mathrm{tg}\beta > 1$. For large $M_{H^\pm}$ and $\mathrm{tg}\beta$ values, the top–bottom decay mode $H^+ \to t\bar{b}$ becomes dominant.

Adding up the various decay modes, the width of all five Higgs bosons remains very narrow, being of order 1 GeV even for large masses.

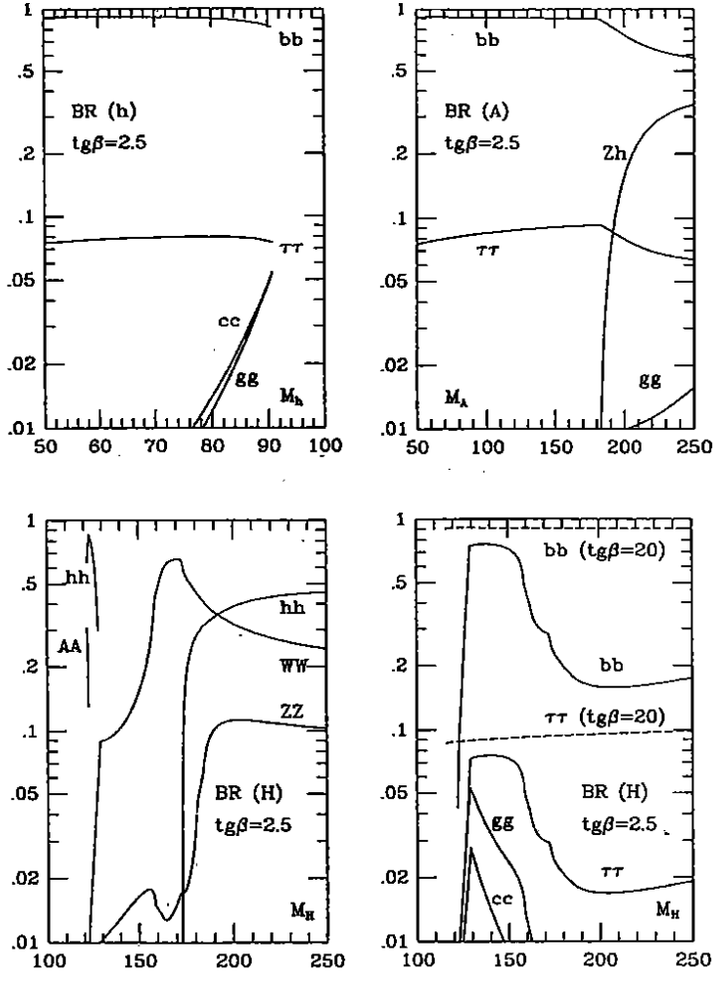


**Fig. 15:** **(a–c)** *Decay branching ratios of the $\mathcal{CP}$-even neutral $\mathcal{MSSM}$ Higgs bosons as a function of their masses for the value* $\mathrm{tg}\beta = 2.5$.



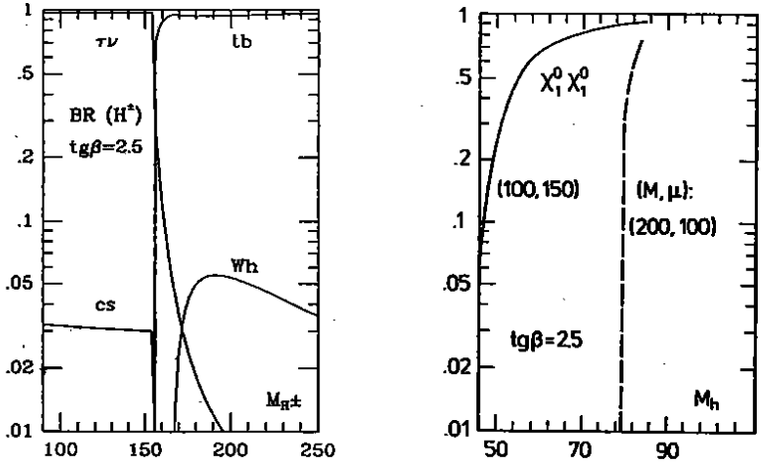


**Fig. 15:** **(d–e)** *Decay branching ratios of the charged Higgs boson ($\mathrm{tg}\beta = 2.5$) and invisible decays of the lightest Higgs boson into LSP pairs.*

Production Processes

The search for the neutral $\mathcal{SUSY}$ Higgs bosons at 500 GeV $e^+e^-$ colliders will be a direct continuation of the search to be performed at LEP200. This collider is expected to cover the mass range up to $\sim 85$ GeV for neutral Higgs bosons. Higher energies, $\sqrt{s} \sim 240$ GeV, are required to sweep the entire parameter space of the $\mathcal{MSSM}$. The main production mechanisms of neutral Higgs bosons at $e^+e^-$ colliders [62,60] are the bremsstrahl process and pair production,

(*a*) bremsstrahlung $\quad e^+e^- \to (Z) \to Z + h/H$
(*b*) pair production $\quad e^+e^- \to (Z) \to A + h/H$

as well as the fusion processes,

(*c*) fusion processes $\quad e^+e^- \to \nu\,\bar{\nu}\,(WW) \to \nu\,\bar{\nu} + h/H$
$\qquad\qquad\qquad\qquad\quad e^+e^- \to e^+e^-(ZZ) \to e^+e^- + h/H$

The $\mathcal{CP}$–odd Higgs boson $A$ cannot be produced in fusion processes to leading order.

The cross sections for the four bremsstrahl and pair production processes can be expressed as

$$\sigma(e^+e^- \to Zh) = \sin^2(\beta-\alpha)\ \sigma_{SM}$$
$$\sigma(e^+e^- \to ZH) = \cos^2(\beta-\alpha)\ \sigma_{SM}$$
$$\sigma(e^+e^- \to Ah) = \cos^2(\beta-\alpha)\ \sigma_{SM}\ \bar{\lambda}$$
$$\sigma(e^+e^- \to AH) = \sin^2(\beta-\alpha)\ \sigma_{SM}\ \bar{\lambda}$$

where $\sigma_{SM}$ is the $\mathcal{SM}$ cross section for Higgs bremsstrahlung and the factor $\bar{\lambda} \sim \lambda_{Aj}^{3/2}/\lambda_{Zj}^{1/2}$ accounts for the correct suppression of the $P$–wave cross sections near the threshold. The cross sections for the bremsstrahlung and for the pair production as well as the cross sections for the production of the light and the heavy neutral Higgs bosons $h$ and $H$ are mutually complementary to each other, coming either with a coefficient $\sin^2(\beta-\alpha)$ or $\cos^2(\beta-\alpha)$. As a result, since $\sigma_{SM}$ is large, at least the lightest $\mathcal{CP}$–even Higgs boson must be detected.

The cross sections for the various production mechanisms of the neutral Higgs bosons are shown as functions of the Higgs mass in Fig. 16, for $\mathrm{tg}\beta = 20$. The cross section for $hZ$ is large for large values of $M_h$ where it is of the order of $\sim 50$ fb, corresponding to $\sim 500$ events for an integrated luminosity of 10 fb$^{-1}$. By contrast, the cross section for $HZ$ is large for light $h$ [implying small $M_H$]. In the case of $h$ [and also for $H$ in most of the parameter space] the signal consists of a $Z$ boson accompanied by a $b\bar{b}$ or a $\tau^+\tau^-$ pair. The signal is easy to separate from the background which comes mainly from $ZZ$ production if the Higgs mass is close to $M_Z$. For the associated channels $e^+e^- \to Ah$ and $AH$, the situation is opposite to the previous case: The cross section for $Ah$ is large for light $h$ whereas $AH$ production is preferred in the complementary region. The sum of the two cross sections decreases from $\sim 50$ to 10 fb if $M_A$ increases from $\sim 50$ to 200 GeV. In major parts of the parameter space, the signals consist of four $b$ quarks in the final state, requiring facilities for efficient $b$ quark tagging. Mass constraints will help to eliminate the backgrounds from QCD jets as well as $ZZ$ final states. For the $WW$ fusion mechanism, the cross sections are larger than for the bremsstrahl process if the Higgs mass is moderately small — less than 160 GeV at $\sqrt{s} = 500$ GeV. However, since the final state cannot be fully reconstructed, the signal is more difficult to extract. As in the case of the bremsstrahl process, the production of light $h$ and heavy $H$ Higgs bosons are complementary. The cross sections for the $ZZ$ fusion mechanism are about an order of magnitude smaller than for the $WW$ fusion process. $ZZ$ fusion will nevertheless be useful since the final state can be fully reconstructed.

An interesting problem is the discrimination of the negative parity of the pseudoscalar Higgs boson $A$ from the positive parity of the Higgs bosons $h, H$. Since $A$ couples to the $Z$ boson only through loops, the rate $e^+e^- \to ZA$ is too small to exploit the angular distribution of this process in practice. However, $\gamma\gamma$ collisions appear to



provide a viable alternative [63]. The fusion of Higgs particles in linearly polarized photon beams depends on the angle between the polarization vectors. For scalar particles the production amplitude $\sim \vec{\varepsilon}_1 \cdot \vec{\varepsilon}_2$ is non–zero only for parallel vectors while pseudoscalar particles with amplitudes $\sim \vec{\varepsilon}_1 \times \vec{\varepsilon}_2$ require perpendicular polarization vectors. For typical experimental set–ups for Compton back–scattering of laser light, the maximum degree of linear polarization of the generated hard photon beams is less than about 30% so that the efficiency for two polarized beams is reduced to less than 10%. This method therefore requires high luminosities, and, moreover, a careful analysis of background rejection due to the enormous number of $b\bar{b}$ pairs produced in $\gamma\gamma$ collisions.

The charged Higgs bosons, if lighter than the top quark, can be produced in top decays, $t \to b + H^+$, with a branching ratio varying between 2% and 20% in the kinematically allowed region. Since the cross section for top pair production is of order 0.5 pb at $\sqrt{s} = 500$ GeV, this corresponds to 200 to 2000 charged Higgs bosons at a luminosity $\int \mathcal{L} = 10\, fb^{-1}$. Since for $\mathrm{tg}\beta$ larger than unity, the charged Higgs bosons will decay mainly into $\tau\nu_\tau$, this results in a surplus of $\tau$ final states over $e, \mu$ final states in $t$ decays, an apparent breaking of lepton universality. For large Higgs masses the dominant decay mode is the top decay $H^+ \to t\bar{b}$. In this case the charged Higgs particles must be pair produced in colliders:

$$e^+e^- \to H^+H^-$$

The cross section depends only on the charged Higgs mass [and does not depend on any extra parameter]. For small Higgs masses the cross section is of order 100 fb, but it drops very quickly due to the $P$–wave suppression $\sim \beta^3$ near the threshold. For $M_{H\pm} = 220$ GeV, the cross section falls to a level of $\simeq 5\, fb$, which for an integrated luminosity of $10\, fb^{-1}$ corresponds to 50 events. Search strategies have been investigated in Ref. [64].

The preceding discussion of the $\mathcal{MSSM}$ Higgs sector at $e^+e^-$ linear colliders can be summarized in the following points [Fig. 16]:

($i$) The lightest $\mathcal{CP}$–even Higgs particle $h$ can be detected in the entire range of the $\mathcal{MSSM}$ parameter space, either through the bremsstrahl process $e^+e^- \to hZ$ or through pair production $e^+e^- \to hA$. In fact, this conclusion holds true even at a c.m. energy of 300 GeV, independently of the top and squark mass values, and also if invisible neutralino decays are allowed for.

($ii$) There is a substantial area of the $[M_h, \mathrm{tg}\beta]$ parameter space where *all* $\mathcal{SUSY}$ Higgs bosons can be discovered at a 500 GeV collider. This is possible if the masses of the heavy scalar $H$, the pseudoscalar $A$ boson and the charged Higgs boson $H^\pm$ are less than $\sim 230$ GeV.

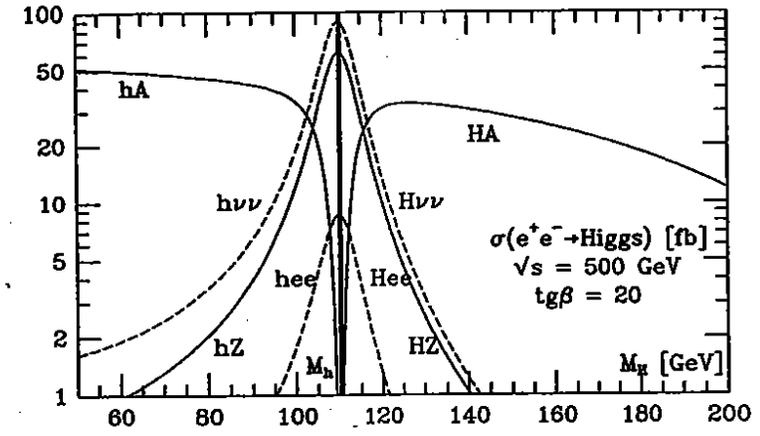


**Fig. 16:** (a) *Production cross sections of the SUSY neutral Higgs bosons in $e^+e^-$ collisions as a function of the masses [in GeV] for* $\mathrm{tg}\beta = 20$.

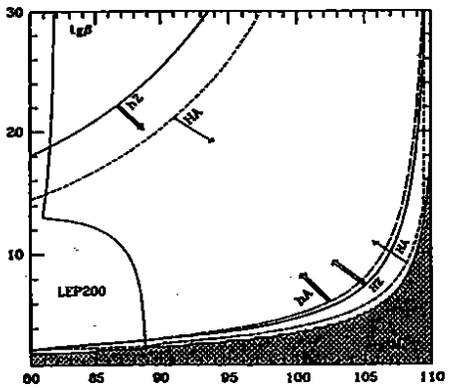


**Fig. 16:** (b) *Regions of the $[M_h, \mathrm{tg}\beta]$ plane where the four cross sections are larger than 2.5 fb [50 events for $\int \mathcal{L} = 20\ fb^{-1}$]. The dashed area is the theoretically forbidden region. The thin lines are the regions which can be probed at LEP200 [25 events at $\sqrt{s} = 180$ GeV and $\int \mathcal{L} = 500\ pb^{-1}$].*



(*iii*) In some part of the $\mathcal{MSSM}$ parameter space, the lightest Higgs particle $h$ can be detected but it cannot be distinguished from the $SM$ Higgs boson. This happens if, for a given value of $\mathrm{tg}\beta$, $M_h$ is very close to its maximum. Then $H$, $A$ and $H^\pm$ are too heavy to be produced in association and deviations of $BR(h \to b\bar{b})$ from the $\mathcal{SM}$ value are too small to be detected [for $m_A \geq 300$ GeV], since the couplings of $h$ to gauge bosons and fermions become $\mathcal{SM}$ like [65]. Virtual effects of supersymmetric particles on the $h$ couplings to $\mathcal{SM}$ particles are in general rather small.

## 5. Supersymmetric Particles

Even though there is no experimental evidence so far for the realization of supersymmetry in nature, this concept has so many attractive features that it may be considered as one of the prime targets of present and future experimental particle research. Arguments in favor of supersymmetry are deeply rooted in particle physics. Supersymmetry is the most general symmetry of the S matrix in quantum field theory and it may play an important role in a quantum theory of gravity. In relating particles of different spins to each other, fermions and bosons, low–energy supersymmetry, broken at the electroweak scale, stabilizes the masses of fundamental Higgs scalars in the context of very high energy scales associated with grand unification. Besides solving this hierarchy problem, supersymmetry may even be closely related to the physical origin of the Higgs phenomenon itself. In a supergravity inspired GUT realization with universal scalar masses at the GUT scale, the evolution of one of the scalar masses squared can become negative and thus lead to spontaneous symmetry breaking if the top mass has a value between about 100 to 200 GeV while all other masses squared of squarks and sleptons remain positive.

The minimal supersymmetric extension of the Standard Model is based on the $\mathcal{SM}$ group $SU(3) \times SU(2) \times U(1)$. The gauginos are the supersymmetric spin–$\frac{1}{2}$ partners of the gauge bosons. The quark and lepton matter particles are associated with scalar supersymmetric particles, squarks and sleptons. To preserve supersymmetry, two Higgs doublets are needed, the supersymmetric partners of which are spin–$\frac{1}{2}$ Higgsinos. Supersymmetric partners carry a multiplicative quantum number $R = -1$ ($R = +1$ for ordinary particles) which is conserved in this model. Supersymmetric particles are therefore generated in pairs and the lightest state $LSP$ is stable.

In the GUT related formulation of the theory, four parameters specify basically the supersymmetric particle sector. The scalar mass parameter $m_0$, the $SU(2)$ gaugino mass $M$, the coupling $\mu$ of the Higgs doublets in the superpotential, and $\tan\beta$, the ratio of the vacuum expectation values $v_2/v_1$. $M$ is related to the gluino mass by

$M/m_{\tilde{g}} \approx \alpha_2/\alpha_3 \approx 0.3$. The Higgs sector requires another parameter which is in general identified with the mass of the pseudoscalar Higgs boson $m_A$. Evolving the scalar masses from the GUT scale down to low energies, it turns out that non–colored particles are significantly lighter than colored particles. A range of mass values, compatible with present low–energy high–precision data and based on the requirement of no unnatural fine–tuning, is shown in the following table. The non–colored Winos and charged Higgsinos mix in general to form the chargino mass eigenstates $\tilde{\chi}_i^{\pm}(i = 1,2)$ while the Zinos and neutral Higgsinos form the neutralinos $\tilde{\chi}_i^0(i = 1,\ldots,4)$.

| Parameters | $m_{1/2}$ | 140 | 230 |
|---|---|---|---|
| | $m_0$ | 190 | 120 |
| | $\mu_0$ | 190 | —120 |
| | $m_t$ | 160 | 100 |
| | $\tan\beta$ | 21 | 5 |
| Gauginos | $\tilde{\gamma}$ | 57 | 83 |
| | $\tilde{Z}$; $\tilde{W}$ | 99; 99 | 120; 112 |
| | $\tilde{g}$ | 354 | 559 |
| Sleptons | $\tilde{l}_L$ | 220 | 206 |
| | $\tilde{l}_R$ | 195 | 146 |
| Squarks | $\tilde{u}_L$, $\tilde{c}_L$; $\tilde{d}_L$, $\tilde{s}_L$ | 365; 373 | 511; 517 |
| | $\tilde{u}_L^c$, $\tilde{c}_R^c$ | 359 | 495 |
| | $\tilde{d}_R^c$, $\tilde{s}_R^c$, $\tilde{b}_R$ | 358 | 491 |
| | $\tilde{t}_L$; $\tilde{b}_L$ | 325; 335 | 491; 497 |
| | $\tilde{t}_R^c$ | 273 | 452 |
| Higgs & Higgsinos | $H^0$ | 91, 264 | 84, 221 |
| | $H^{\pm}$; $A^0$ | 276; 264 | 232; 218 |
| | $\widetilde{H}^0$ | 205, 225 | 139, 226 |
| | $\widetilde{H}^{\pm}$ | 229 | 227 |

**Table 2:** *Estimate of possible mass ranges of supersymmetric particles [66] based on present high–precision data and the requirement of no fine–tuning; masses in GeV; see also Refs. [20,67].*

Support for a spectrum of the $\mathcal{MSSM}$ in the mass range of several hundred GeV follows from the measurement of the electroweak mixing angle $\sin^2\vartheta_W$ [68]. The value $\sin^2\vartheta_W = 0.2334 \pm 0.0026$ predicted by the $\mathcal{MSSM}$ is matched surprisingly well by the present experimental value $\sin^2\vartheta_W = 0.2324 \pm 0.0006$.



## 5.1 Gauginos and Higgsinos

The two charginos $\tilde{\chi}_i^+$ and the four neutralinos $\tilde{\chi}_i^0$, mixtures of the [non–colored] gauginos and Higgsinos, are expected to be the lightest supersymmetric particles. In the $\mathcal{MSSM}$ with conserved $R$–parity, the neutralino $\tilde{\chi}_1^0$ with the smallest mass, assumed to be the lightest supersymmetric particle altogether, is stable. The heavier neutralinos and the charginos decay into (possibly virtual) gauge and Higgs bosons plus the $LSP$, $\tilde{\chi}_i^0 \longrightarrow \tilde{\chi}_1^0 + Z$ and $\tilde{\chi}_1^0 + W$, or if they are heavy enough, into neutralino/chargino cascades, and leptons plus sleptons [69].

Neutralinos and charginos are difficult to observe at hadron colliders, but they are easy to detect at $e^+e^-$ colliders. They are produced in pairs

$$e^+e^- \longrightarrow \tilde{\chi}_i^+ + \tilde{\chi}_j^- \qquad [i,j = 1,2]$$
$$e^+e^- \longrightarrow \tilde{\chi}_i^0 + \tilde{\chi}_j^0 \qquad [i,j = 1,..,4]$$

through $s$–channel $\gamma, Z$ exchange and $t$–channel selectron or sneutrino exchange. The kinematically accessible $\mathcal{SUSY}$ parameter range in the $[M,\mu]$ plane for various chargino and neutralino pairs is shown in Fig. 17, for various chargino and neutralino production processes at a 500 GeV $e^+e^-$ collider. Compared to the region which can be explored by LEP200, a substantial extension can be expected. Since the cross sections are as large as $\mathcal{O}$(100 fb), enough events will be produced to discover these particles for masses nearly up to the kinematical limit. It has been demonstrated by detailed experimental simulations, in fact, that these particles can be found with masses up to the beam energy if the mass difference $m(\tilde{\chi}) - m(\tilde{\chi}_1^0)$ is not less than about 20 GeV [70].

The properties of the neutralinos and charginos can be studied at great detail in $e^+e^-$ collisions. From the fast onset $\sim \beta$ of the excitation curve near the threshold, the masses can be measured very accurately within a few hundred MeV. The decay spectrum in $\tilde{\chi}_1^+ \rightarrow \tilde{\chi}_1^0 + W^+$ allows us to measure the mass of the $LSP$ within $\pm$ 2 GeV, Fig. 18. Using polarized $e^{\pm}$ beams, the decomposition of the states, $\tilde{\chi}_1^+ = \alpha\tilde{W}^+ + \beta\tilde{H}^+$ into Wino and Higgsino components can be determined since left–handed electrons couple to sneutrinos in the $t$–channel but right–handed electrons do not, so that the energy and angular dependence of the cross sections will be different [71].

## 5.2 Sleptons

The superpartners of the right–handed leptons decay into the associated $\mathcal{SM}$ partners and neutralinos/charginos. In major parts of the $\mathcal{SUSY}$ parameter space the

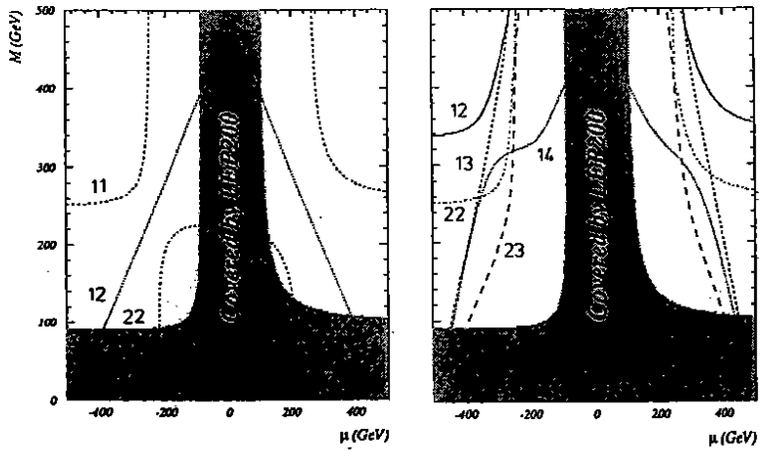


**Fig. 17**: *Regions of the $[\mu, M]$ plane for $\mathrm{tg}\beta = 4$ where the processes $e^+e^- \to \tilde{\chi}_i^+\tilde{\chi}_j^-$ and $e^+e^- \to \tilde{\chi}_i^0\tilde{\chi}_j^0$ are kinematically accessible at $\sqrt{s} = 500$ GeV. The labels $ij$ correspond to $\tilde{\chi}_i\tilde{\chi}_j$ combinations; from Ref. [69].*

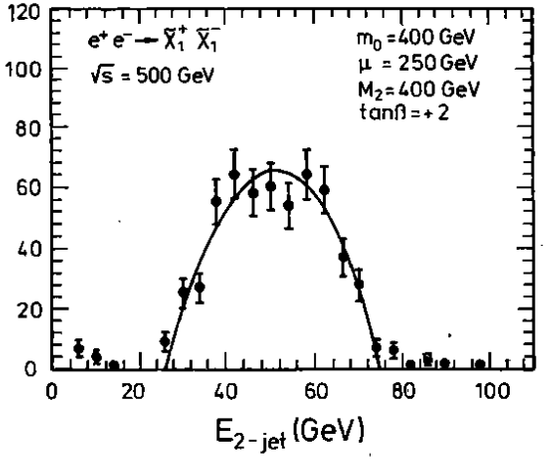


**Fig. 18**: *Energy spectrum of the $2j$ decay products in $\tilde{\chi}_i^+ \to \tilde{\chi}_i^0 + W^+, W^+ \to jj$; from Ref.[71].*



dominant decay mode is $\tilde{\mu}_R \to \mu + \tilde{\chi}_1^0$ [69,72,73]. For the superpartners of the left–handed sleptons, the decay pattern is slightly more complicated since besides the $\tilde{\chi}_1^0$ channels, decays into leptons and charginos are also possible. In $e^+e^-$ collisions, sleptons are produced in pairs

$$e^+e^- \longrightarrow \tilde{\mu}_L^+\tilde{\mu}_L^- \ , \ \tilde{\mu}_R^+\tilde{\mu}_R^- \ , \ \tilde{\tau}_L^+\tilde{\tau}_L^- \ , \ \tilde{\tau}_R^+\tilde{\tau}_R^-$$
$$e^+e^- \longrightarrow \tilde{e}_L^+\tilde{e}_L^- \ , \ \tilde{e}_R^+\tilde{e}_R^- \ , \ \tilde{e}_L^+\tilde{e}_R^- \ , \ \tilde{e}_R^+\tilde{e}_L^-$$
$$e^+e^- \longrightarrow \tilde{\nu}_L\bar{\tilde{\nu}}_L$$

For charged sleptons, the production proceeds via $\gamma, Z$ exchange in the $s$–channel. In the case of selectrons, an additional $t$–channel neutralino exchange, which is also responsible for the creation of the mixed left and right–handed selectron states, is present, Fig. 19. For sneutrinos, the process is mediated by $s$–channel $Z$–exchange and, in the case of electron–sneutrinos, also by $t$–channel exchange of charginos.

The cross sections for the pair production of sleptons are of the order of $10^{-1}$ to $10^{-2}$ pb so that their discovery is very easy up to the kinematical limit. Enough events will be produced to study their detailed properties. The polarization of the $e^\pm$ beams will help considerably to identify the couplings of these particles. From the decay spectra the mass of the $LSP$ can be determined up to a level of $\pm 1$ GeV [71], Fig. 20.

Selectrons can also be produced in association with photinos [$\sim \tilde{\chi}_1^0$] in $e\gamma$ collisions,

$$e\gamma \to \tilde{e}\tilde{\chi}_1^0$$

For small photino masses, the kinematic range of the selectron mass extends beyond the $e^\pm$ beam energy [74]. However, it seems difficult to exploit this window in practice, since for masses beyond the $e^\pm$ beam energies the rates are quite low.

If one of the stop states is light enough due to the strong $LR$ Yukawa mixing, also these particles may be pair produced at a 500 GeV collider. By measuring the $LR$ asymmetry of the production cross sections, the $\tilde{t}_L/\tilde{t}_R$ mixing angle can be determined [75].

While colored squarks and gluinos can be detected up to $\mathcal{O}(1$ TeV) at proton colliders, the search for sleptons at these colliders is very difficult, on the other hand, due to the low production rates and the large backgrounds so that $e^+e^-$ colliders are unique facilities in this sector.

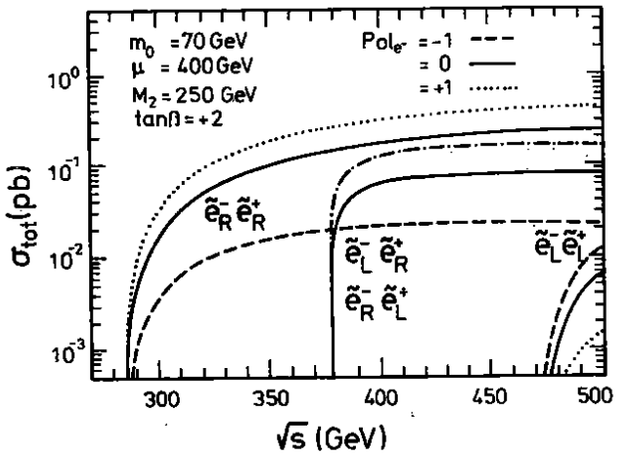


**Fig. 19**: *Production of selectrons in polarized $e^{\pm}$ beams; from Ref.[71].*

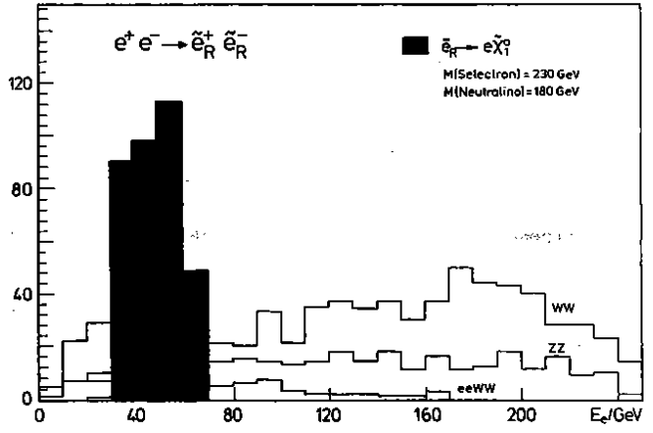


**Fig. 20**: *Energy distribution of the decay electrons in selectron production. The signal is compared with the main background processes; Ref.[72].*



## REFERENCES


[1] Proceedings, $e^+e^-$ *Collisions at 500 GeV: The Physics Potential*, Munich-Annecy-Hamburg 1990/91, P.M. Zerwas ed., DESY 92-123A+B.

[2] Proceedings, *Physics and Experiments with $e^+e^-$ Linear Colliders*, Saariselkä 1991, R. Orava, P. Eerola and M. Nordberg eds., World Scientific, Singapore 1992.

[3] JLC - I, JLC Group, S. Matsumoto et al., KEK Report 92-16.

[4] B. Wiik in Ref. [2], and Proceedings of the EPS Conference on High Energy Physics, Marseille 1993.

[5] B. Richter in Ref. [2].

[6] J. Rossbach, Talk at *The 1992 Linear Accelerator Conference, Ottawa*, Internal Report DESY M-93-01; for details see *LC92-ECFA Workshop on $e^+e^-$ Linear Colliders*, R. Settles ed., MPI-PhE/93-14 and ECFA 93-154.

[7] H.F. Ginzburg, G.L. Kotkin, S.L. Panfil, V.G. Serbo and V.I. Telnov, Nucl. Instr. and Meth. 219 (1984) 5.

[8] S.J. Brodsky, Proceedings of 1993 Hawaii Workshop on Physics with $e^+e^-$ Linear Colliders.

[9] C.A. Heusch and P. Minkowski, Proceedings of 1993 Hawaii Workshop on Physics with $e^+e^-$ Linear Colliders.

[10] D. Schaile and P.M. Zerwas, Phys. Rev. D45 (1992) 3262;
update by D. Schaile, private communication.

[11] J. Lefrancois, Proceedings of the EPS Conference on High Energy Physics, Marseille 1993.

[12] A. Barbiero-Galtieri, Proceedings of the EPS Conference on High Energy Physics, Marseille 1993.

[13] I. Bigi, Yu. Dokshitzer, V. Khoze, J. Kühn and P.M. Zerwas, Phys. Lett. 181B (1986) 157.

[14] M. Jezabek and J.H. Kühn, Karlsruhe Report TTP-93-4.

[15] K. Fujii in Ref. [2].

[16] V.A. Khoze, W.J. Stirling and L.H. Orr, Nucl. Phys. B378 (1992) 413.

[17] Y. Sumino, Proceedings of 1993 Hawaii Workshop on Physics with $e^+e^-$ Linear Colliders.

[18] P.M. Zerwas, *Top Quark Physics*, in Ref. [2]

[19] J.L. Hewett, Phys. Rev. Lett. 70 (1993) 1045;
V. Barger, M.S. Berger and R.J.N. Phillips, Phys. Rev. Lett. 70 (1993) 1368.

[20] F. Borzumati, DESY Report 93–090.

[21] W.S. Hou, Phys. Lett. B296 (1992) 179;
L.J. Hall and S. Weinberg, Phys. Rev. D48 (1993) 979.

[22] J. Jersak, E. Laermann and P.M. Zerwas, Phys. Rev. D25 (1982) 363.

[23] G.L. Kane, G.A. Ladinsky and C.–P. Yuan, Phys. Rev. D45 (1992) 124.

[24] M.E. Peskin and C. Schmidt in Ref. [2].

[25] W. Bernreuther et al., in *Top Quark Physics*, Ref. [1].

[26] O. Podobrin, Proceedings, $e^+e^-$ *Collisions at 500 GeV: The Physics Potential*, Munich–Annecy–Hamburg 1992/93, DESY 93–123C.

[27] J.H. Kühn, Acta Phys. Austr. Suppl. 24 (1982) 203.

[28] V.S. Fadin and V.A. Khoze, JETP Lett. 46 (1987) 525 and Sov. J. Nucl. Phys. 48 (1988) 309.

[29] M.J. Strassler and M.E. Peskin, Phys. Rev. D43 (1991) 1500.

[30] Y. Sumino, K. Fujii, K. Hagiwara, M. Murayama and C.K. Ng, Phys. Rev. D47 (1993) 56;
M. Jezabek, J.H. Kühn and T. Teubner, Z. Phys. C56 (1992) 653;
M. Jezabek and T. Teubner, Karlsruhe Preprint TTP 92–38.

[31] P. Igo-Kemenes, M. Martinez, R. Miquel and S. Orteu, Proceedings, $e^+e^-$ *Collisions at 500 GeV: The Physics Potential*, Munich–Annecy–Hamburg 1992/93, DESY 93–123C.

[32] P. Igo-Kemenes, Proceedings of 1993 Hawaii Workshop on Physics with $e^+e^-$ Linear Colliders.

[33] M. Claudson, E. Farhi and R.L. Jaffe, Phys. Rev. D34 (1986) 873;
S.J. Brodsky and J.R. Hiller, Phys. Rev. D46 (1992) 931.

[34] F. Boudjema in Ref.[1].



[35] G. Gounaris, J. L. Kneur, J. Layssac, G. Moultaka, F. M. Renard and D. Schildknecht in Ref. [1].

[36] T. Barklow in Ref. [2].

[37] W. Buchmüller and D. Wyler, Nucl. Phys. B268 (1986) 621.

[38] K. Hagiwara, S. Ishihara, R. Szalapski and D. Zeppenfeld, Phys. Lett. B283 (1992) 353.

[39] A. Miyamoto, Proceedings of 1993 Hawaii Workshop on Physics with $e^+e^-$ Linear Colliders.

[40] A. Falk, M. Luke and E.H. Simmons, Nucl. Phys. B365 (1991) 523.

[41] T. Barklow, Proceedings of 1993 Hawaii Workshop on Physics with $e^+e^-$ Linear Colliders.

[42] L. Okun, *Leptons and Quarks*, North Holland Pub. Comp. 1982.

[43] K. Hikasa in Ref.[2], and references therein. See also Y. Kurihara and R. Najima, KEK Preprint 93–90; and Y. Kurihara, KEK Preprint 93–114.

[44] T. Barklow in Ref. [2].

[45] J.L. Hewett, Proceedings of 1993 Hawaii Workshop on Physics with $e^+e^-$ Linear Colliders.

[46] A. Djouadi, A. Leike, T. Riemann, D. Schaile and C. Verzegnassi, Z. Phys. C56 (1992) 289.

[47] J.L. Hewett and T.G. Rizzo, in Ref. [2] and Int. J. Mod. Phys. A4 (1989) 4551.

[48] N. Paver, Proceedings, $e^+e^-$ *Collisions at 500 GeV: The Physics Potential*, Munich–Annecy–Hamburg 1992/93, DESY 93–123C.

[49] V. Barger et al., Phys. Rev. D33 (1986) 1912;
T.G. Rizzo, Phys. Rev. D34 (1986) 1438;
F. del Aguila, E. Laermann and P.M. Zerwas, Nucl. Phys. B297 (1988) 1;
W. Buchmüller and C. Greub, Nucl. Phys. B363 (1991) 345;
A. Djouadi, M. Spira and P.M. Zerwas in Ref. [1];
W. Buchmüller, C. Greub, P. Mikowski, M. Talbi and G. Tysarcszyk–Niemeyer in Ref. [1];
F. Csikor, A. Djouadi and I. Montvay in Ref. [1].

[50] N. Cabibbo, L. Maiani, G. Parisi and R. Petronzio,
Nucl. Phys. B158 (1979) 295;
M. Chanowitz, M. Furman and I. Hinchliffe, Phys. Lett. B78 (1978) 285;
R.A. Flores and M. Sher, Phys. Rev. D27 (1983) 1679;
M. Sher, Phys. Rep. 179 (1989) 273;
M. Lindner, Z. Phys. C31 (1986) 295.

[51] D. Haidt et al. in Ref. [1];
J.F. Gunion and P. Janot, Proceedings of 1993 Hawaii Workshop on Physics with $e^+e^-$ Linear Colliders.

[52] V. Barger, K. Cheung, R.J.N. Phillips and B.A. Kniehl, Phys. Rev. D46 (1992) 3725.

[53] V. Barger, K. Cheung, A. Djouadi, B.A. Kniehl and P.M. Zerwas, DESY 93–064 and Phys. Rev. D in print.

[54] See also E. Boos, M. Sachwitz, H.J. Schreiber and S. Shichanin, DESY 93–089.

[55] P. Grosse–Wiesmann, D. Haidt and J. Schreiber in Ref. [1];
P. Janot in Ref. [51].

[56] M. Hildreth, Proceedings of 1993 Hawaii Workshop on Physics with $e^+e^-$ Linear Colliders.

[57] A. Djouadi, J. Kalinowski and P.M. Zerwas, Mod. Phys. Lett. A7 (1992) 1765 and Z. Phys. C54 (1992) 255.

[58] K. Hagiwara, H. Murayama and I. Watanabe, Nucl. Phys. B367 (1991) 257.

[59] Y. Okada, M. Yamaguchi and T. Yanagida, Prog. Theor. Phys. 85 (1991) 1;
H. Haber and R. Hempfling, Phys. Rev. Lett. 66 (1991) 1815;
J. Ellis, G. Ridolfi and F. Zwirner, Phys. Lett. 257B (1991) 83;
R. Barbieri, F. Caravaglios and M. Frigeni, Phys. Lett. 258B (1991) 167;
J. Gunion and A. Turski, Phys. Rev. D39 (1989) 2701 and D40 2333;
M. Berger, Phys. Rev. D41 (1990) 225;
P. H. Chankowski, S. Pokorski and J. Rosiek, Phys. Lett. 274B (1992) 191;
A. Yamada, Phys. Lett. 263B (1991) 233;
J. R. Espinosa and M. Quiros, Phys. Lett. 266B (1991) 389;
M. Drees and M. N. Nojiri, Phys. Rev. D45 (1992) 2482;
P.H. Chankowski, S. Pokorski and J. Rosiek, Phys. Lett. 274B (1992) 191.

[60] A. Djouadi, J. Kalinowski and P.M. Zerwas, Z. Phys. C57 (1993) 569.

[61] J.C. Ramao et al., Proceedings, $e^+e^-$ *Collisions at 500 GeV: The Physics Potential*, Munich–Annecy–Hamburg 1992/93, DESY 93–123C.



[62] J.F. Gunion et al., Phys. Rev. D38 (1988) 3444.

[63] J. Grzadkowski and J.F. Gunion, Phys. Lett. B294 (1992) 361.

[64] P. Eerola and J. Sirkka in Ref. [1];
A. Sopczak, Proceedings of 1993 Hawaii Workshop on Physics with $e^+e^-$ Linear Colliders.

[65] P. Janot in Ref. [51].

[66] G.G. Ross and R.G. Roberts, Nucl. Phys. B377 (1992) 571.

[67] R.G. Roberts and L. Roszkowski, Phys. Lett. B390 (1993) 329;
M. Olechowski and S. Pokorski, MPI–Ph/92–118;
W. de Boer, R. Ehret and D.I. Kazakov, IEKP–KA/93–12.

[68] J. Ellis, S. Kelley and D. V. Nanopoulos, Phys. Lett. 260B (1991) 131;
U. Amaldi, W. de Boer and H. Fürstenau, Phys. Lett. 260B (1991) 447;
P. Langacker and M. Luo, Phys. Rev. D44 (1991) 817.

[69] A. Bartl, W. Majerotto and B. Mösslacher in Ref. [1].

[70] F. Grivaz in Ref. [2].

[71] T. Tsukamoto and S. Orito, Proceeding of 1993 Hawaii Workshop on Physics with $e^+e^-$ Linear Colliders.

[72] C. Vander Velde in Ref. [1]

[73] R. Becker and R. Starosta in Ref. [1].

[74] D. Borden, D. Bauer and D. Caldwell, SLAC–PUB–5715 (1992);
H. König and K. Peterson, Phys. Lett. B294 (1992) 110;
F. Cuypers, G. van Oldenborgh and R. Rückl, Nucl. Phys. B383 (1992) 45.

[75] T. Kon, Proceedings of 1993 Hawaii Workshop on Physics with $e^+e^-$ Linear Colliders.